LBNL-42625
Preprint

ERNEST ORLANDO LAWRENCE
BERKELEY NATIONAL LABORATORY

Global Earth Structure: Inference and Assessment

D.W. Vasco, Lane R. Johnson,
and Osni Marques

Computing Sciences Directorate
National Energy Research
Scientific Computing Center

November 1998

Submitted to
Geophysical Journal International

REFERENCE COPY
Does Not
Circulate
Bldg. 50 Library - Ref.
Lawrence Berkeley National Laboratory

LBNL-42625
Copy 1

DISCLAIMER

This document was prepared as an account of work sponsored by the United States Government. While this document is believed to contain correct information, neither the United States Government nor any agency thereof, nor the Regents of the University of California, nor any of their employees, makes any warranty, express or implied, or assumes any legal responsibility for the accuracy, completeness, or usefulness of any information, apparatus, product, or process disclosed, or represents that its use would not infringe privately owned rights. Reference herein to any specific commercial product, process, or service by its trade name, trademark, manufacturer, or otherwise, does not necessarily constitute or imply its endorsement, recommendation, or favoring by the United States Government or any agency thereof, or the Regents of the University of California. The views and opinions of authors expressed herein do not necessarily state or reflect those of the United States Government or any agency thereof or the Regents of the University of California.

LBNL-42625

Global Earth Structure: Inference and Assessment

D.W. Vasco,* Lane R. Johnson,* and Osni Marques**

*Center for Computational Seismology
Ernest Orlando Lawrence Berkeley National Laboratory
University of California
Berkeley, California 94720

**Computing Sciences Directorate
National Energy Research Scientific Computing Center
Ernest Orlando Lawrence Berkeley National Laboratory
University of California
Berkeley, California 94720

November 1998

This work was supported by a Laboratory Directed Research and Development grant and the Director, Office of Computational and Technology Research, Division of Mathematical, Information, and Computational Sciences, of the U.S. Department of Energy under Contract No. DE-AC03-76SF00098. Support was also provided by the Defense Special Weapons Agency under Grant No. DSWA-01-97-1-0026.

Submitted to the *Geophysical Journal International*, 1998.

Global Earth structure: Inference and assessment

D. W. Vasco[1] and Lane R. Johnson[1]
Center for Computational Seismology, Berkeley Laboratory, University of California, Berkeley, California

Osni Marques
National Energy Research Scientific Computing Center, Berkeley Laboratory, University of California, Berkeley, California

Abstract

A suite of compressional and shear phase arrival times (P, S, PP, PcP, SS, ScS, $PKPab$, $PKPbc$, $PKPdf$, $SKSac$) and two sets of differential times ($SS - S_{410}S$, $SS - S_{660}S$) are used to infer lateral variations in P and S velocity structure in the entire Earth (crust, mantle, and core). Volumetric heterogeneity is parameterized by 22 depth layers, each of which is subdivided into a grid of cells. In addition to volumetric heterogeneity, we determine topography on the major internal velocity discontinuities, station corrections, event relocation parameters, and inner core anisotropy, a total of 96,300 unknowns. The model parameters are estimated using an iterative Lanczos algorithm to obtain a partial singular value decomposition. A total of 5,000 Lanczos values and vectors are used to construct model parameter estimates as well as measures of model parameter resolution and covariance. The Lanczos resolution estimates provide lower bounds on conventional SVD-based measures. Throughout most of the mantle we find that regions beneath the continents, particularly in the northern hemisphere, are well resolved. With the exception of Africa, velocity variations are moderately well resolved in that portion of the outer core lying beneath the continents. Velocity heterogeneity is poorly resolved in the inner core where cell dimensions are small and deviations in velocity heterogeneity trade off with variations in anisotropy. Variations in the uppermost mantle (2-3 %) are correlated with surface tectonics, while at greater depths high velocity variations coincide with regions of past and present subduction. The high velocity anomalies extend into the lower mantle though with a reduced amplitude (0.5-1.0 %) until the lowest mantle (2.5 %). At the base of the outer core a large scale pattern of heterogeneity (0.8 %) is observed, slower at the poles. In the inner core we infer peak anisotropy of 2-3 % which varies laterally and with depth. However, the magnitude and distribution of the anisotropy trades off strongly with velocity heterogeneity.

INTRODUCTION

In many ways, models of the three-dimensional seismic structure of the Earth have become increasingly sophisticated. Since the first estimates of lower mantle P velocity variation (Sengupta and Toksoz 1976, Dziewonski et al. 1977, Clayton and Comer 1983) investigators have sought to: (1) improve sampling by the incorporation of additional phases and data, (2) refine their parameterizations in order to obtain better spatial resolution, (3) consider the velocity structure of other regions within the Earth such as the upper mantle and core, and (4) account for other aspects of velocity heterogeneity such as boundary deflections and anisotropy. The great variety of studies is a tribute to the continual accumulation of seismic data at seismological stations around the globe, and a sign of advancements both in instrumentation and data analysis.

The diversity of seismological investigations of velocity heterogeneity (Romanowicz 1991, Iyer and Hirahara 1993, Nolet et al. 1994), with variations in both data and model parameters, leads to an equivalent diversity in the resolution of Earth structure. For example, short period body wave travel times, long period waveforms, free-oscillation spectra, and surface wave dispersion curves all differ in their sensitivity to spatial variations in P and S velocities (Snieder et al. 1991, Li and Romanowicz 1996) . Furthermore, spherical harmonics, cells or blocks, and spherical splines are all valid representations of Earth structure but are not equivalent in terms of their response to truncation, their spatial averaging, and their biases due to inhomogeneous sampling (Trampert and Snieder 1996). This last consideration, inhomogeneous sampling, is of paramount importance in the determination of global Earth structure. It has been recognized for some time that the clustering of seismic sources at plate boundaries and the location of a majority of seismographic stations on continents in the northern hemisphere significantly biases the sampling of Earth structure. Surface waves and free-oscillations are less sensitive to the variations in source-receiver distribution, however these vibrational modes have less lateral and depth resolution than do higher frequency body waves. The net result is a great uneveness in our ability to constrain spatial variations in the Earth's seismic velocity.

Accompanying the progress in seismic imaging there have been significant strides in our ability to model processes in the Earth, such as mantle and core convection. Such numerical simulations can now be used to investigate the formation of plumes (Davies 1990), the interaction of subducting slabs with the velocity discontinuities at 400 and 660 km (Tackley et al. 1993), the influence of mantle convection on continental cratons (Lux et al. 1979, Gurnis and Davies 1986, Gurnis and Zhong 1991, Bunge and Richards 1996), and the generation of the Earth's magnetic field (Glatzmaier and Roberts 1995, 1996). The results of such detailed modeling have been compared to estimates of velocity variations in the mantle. Thus, seismological estimates of global structure are to some extent used to validate mantle convection studies. In particular, several studies have compared the scale length of features in convection models with the scale lengths of heterogeneity derived from seismic estimates of mantle structure (Gurnis and Zhong 1991, Bunge and Richards 1996).

As suggested above, there is a need to determine the spatial extent of features in the Earth. However, the great variability in sampling leads one to suspect that there are corresponding variations in the ability of seismological data to constrain estimates of velocity heterogeneity and the spatial dimensions of the anomalies. If global velocity models are to definitively constrain the scale lengths of features in the Earth they must be accompanied by some estimate of spatial resolution and uncertainty. Unfortunately, with few exceptions (Tanimoto 1986, Vasco et al. 1993), computational considerations have prevented formal estimates of resolution and uncertainty. Rather than estimate resolution and uncertainty directly, most current studies approximate these measures through the inversion of synthetic data sets. One approach is to invert seismic data produced by forward modeling through a structure containing oscillating or 'checkerboard' anomalies. This approach suffers from a dependence on the scale length of the oscillations, as resolution of a long wavelength pattern is different than that of a smaller scale pattern. In fact, in realistic situations, large scale structure may be more poorly resolved than small scale variations (Leveque et al. 1993). Resolution as a function of scale length is quite complicated, depending on the structure of the null-space of the inverse problem (Leveque et al. 1993). Thus, the commonly used checkerboard tests can be quite misleading. The interference between the anomalies of the checkerboard is an additional complication associated with inversions of synthetic data. The estimation of uncertainty involves the inversion of random deviates with the same distribution

as the errors on the data. However, such inversions are dominated by the regularization and do not provide an acceptable estimate of uncertainty (Vasco et al. 1993). For example, in regions of poor coverage, where uncertainty should be large, the inversion of random deviates produces small values due to the regularization.

Several papers have outlined feasible approaches for conducting approximate model assessments for large inverse problems (Scales 1989, Nolet and Snieder 1990, Berryman 1994, Zhang and McMechan 1995, Minkoff 1996, Vasco et al. 1998). The proposed algorithms are well suited for the task of global tomographic imaging and do not suffer the deficiencies associated with inverting synthetic data sets. In this paper we apply an algorithm based upon the Lanczos recursion (Lanczos 1950) to estimate velocity variations in the entire Earth (mantle, outer core, and inner core) and to assess the resulting estimates. We solve for several different types of parameters: P and S velocities, boundary deflections (400 km, 660 km discontinuities, core-mantle boundary, and inner core boundary), stations corrections, hypocentral relocation parameters, and inner core anisotropy, for a total of 96,300 unknowns. Constraining these parameters are 846,968 summary seismic arrival times from 11 different phases which have been gathered by the International Seismological Center (ISC). Because we solve for all classes of parameters and approximate a formal assessment, it is possible to examine spatial resolution in various regions of the Earth, such as the outer core.

METHODOLOGY

In this section we outline the formulation of the inverse problem for Earth structure. Additional details on our particular approach may be found in Pulliam et al. (1993), Vasco et al. (1994, 1995), and Vasco and Johnson (1998). Discussions on seismic tomography in general may be found in Nolet (1987) and Iyer and Hirahara (1993). We also present an overview of techniques for estimating the unknown parameters and assessing our solution, based upon singular value decomposition (SVD). This formalism is well established in geophysics and discussions of greater depth may be found in books on inverse methods (Menke 1984, Parker 1994). A brief section describes the Lanczos recursion and its application to the construction of an approximate model assessment. More information on Lanczos iteration may be found in Cullum and Willoughby (1985), Sehmi (1989), and Berry (1992).

Representation of Earth structure

In order to account for the complexities of wave propagation through the Earth we must consider several classes of parameters. For the sake of illustration, consider a travel time residual for a phase of type l (P,S,PP,$PKPbc$...), observed at station i, associated with earthquake j, δt_{ijl}. Beginning at the source, each event is relocated during the inversion. That is, we solve for shifts in the depth, latitude and longitude of the hypocenter and shifts in the event's origin time contained in the vector $\delta h_j{}^k, k = 1,2,3,4$. Travel times reported to the ISC by individual stations may be biased by several factors (Grand 1990) such as near surface velocity variations, differences in instrumentation, and station mislocation. We include station delays for compressional and shear phases read at each station, denoted by $\delta s_i{}^k, k = 1,2$. Initially (Vasco and Johnson 1998) a station delay was associated with each distinct phase but it was determined that two terms, one for compressional and one for shear phases, recorded by each station produced essentially identical velocity deviation, boundary deflection and anisotropy heterogeneity estimates. Our model of P and S velocity variation consists of 22 layers of 1136 cells each. The lateral dimension of the cells, approximately equal area in a given layer, are 6° by 6° at the equator and the radial extent varies from 35 to 400 km, depending on layer depth (Vasco and Johnson 1998). Velocity is assumed to be constant in each cell and the unknowns represent deviations from the average layer velocity. The radial background P and S velocity models are those of *ak135* (Kennett et al. 1995). The vector of velocity deviations with respect to *ak135* is denoted by $\delta \mathbf{v}$. Because several lines of investigation suggest that the inner core is characterized by an anisotropic velocity structure (Poupinet et al. 1983, Woodhouse et al. 1986, Morelli et al. 1986, Shearer et al. 1988, Creager 1992, Song and Helmberger 1993, Tromp 1993, Vinnik et al. 1994, Song and Richards 1996) we include it in our parameterization. The formulation is similar to that used by Shearer (1994) with expressions obtained from Backus (1965). For cell m in the inner core the velocity is given by

$$v_m(\theta_{ij}) = v^m + a^1{}_m \cos(2\theta_{ij}) + a^2{}_m \cos(4\theta_{ij}) \quad (1)$$

where θ_{ij} is the angle between the tangent to the ray from the jth event to the ith station and the rota-

tion axis, v^m is the isotropic component of velocity. The inner core anisotropy coefficients are collected in the parameter vector $\delta a_m{}^k, k = 1, 2$. There are indications of topography on the major velocity discontinuities in the upper mantle at depths of 410 and 660 km (Shearer and Masters 1992, Shearer 1993). Also a number of studies have produced estimates of depth variations in the core mantle boundary (CMB) (Creager and Jordan 1986, Morelli and Dziewonski 1987, Gudmundsson 1989, Rodgers and Wahr 1993, Obayashi and Fukao 1997). To account for this in our model, we include terms relating perturbations in boundary radius to a travel time deviation. The approach we follow is based upon the derivation of Dziewonski and Gilbert (1976). Further details may be found in Vasco et al. (1995). We consider perturbations induced by structure on the 410 km, the 660 km, the CMB and the inner core boundary (ICB). For boundary element k the depth perturbation is denoted by δb^k.

Robust estimation

Though the relationship between the change in arrival time and the Earth's structural parameters is non-linear, it is thought that the deviations from a purely radial variation are small. Given this assumption a Taylor series expansion, truncated to first order, provides a linear equation relating arrival time deviations to perturbations in Earth structure,

$$\delta t_{ijl} = \sum_{k=1}^{N_{3D}} \frac{\partial t_{ijl}}{\partial v^k} \delta v_l^k + \sum_{k=1}^{4} \frac{\partial t_{ijl}}{\partial h^k} \delta h_j^k + \sum_{k=1}^{N_s} \frac{\partial t_{ijl}}{\partial s^k} \delta s_{il}^k + \sum_{k=1}^{N_b} \frac{\partial t_{ijl}}{\partial b^k} \delta b^k + \sum_{k=1}^{N_a} \frac{\partial t_{ijl}}{\partial a^k} \delta a^k$$

for the lth phase arrival time associated with event j, recorded at station i. The parameter deviations are defined in the previous subsection, the partial derivatives are discussed in our previous papers (Pulliam et al. 1993, Vasco et al. 1994, Vasco et al. 1995, Vasco and Johnson 1998). Given a large collection of arrival times from various source and receiver combinations we can infer variations in Earth structure. The relationship between the vector of travel time deviations ($\delta\mathbf{T}$) and the vector of velocity ($\delta\mathbf{v}$) perturbations, hypo-central location ($\delta\mathbf{h}$) changes, station corrections ($\delta\mathbf{s}$), boundary deflections ($\delta\mathbf{b}$), and variations in inner core anisotropy ($\delta\mathbf{a}$) may be written matrix-vector form

$$\delta\mathbf{T} = \mathbf{V}\delta\mathbf{v} + \mathbf{H}\delta\mathbf{h} + \mathbf{S}\delta\mathbf{s} + \mathbf{B}\delta\mathbf{b} + \mathbf{A}\delta\mathbf{a}. \quad (2)$$

The bold font upper case letters **V**, **H**, **S**, **B**, and **A** represent matrices who's coefficients are the partial derivatives of the travel time with respect to velocity variation, hypo-central re-locations, stations corrections, boundary deflections, and inner core anisotropy deviations, respectively (Pulliam et al. 1993, Vasco et al. 1994, Vasco et al. 1995, Vasco and Johnson 1998).

It is possible to solve the linear system of equations represented by (2) using a least squares technique (Golub and Van Loan 1989, Paige and Saunders 1982). Because of the excessive number of outliers often found in travel time data sets, the basic assumption underlying the least squares algorithm (normally distributed errors) may be violated (Jeffreys 1932, Pulliam et al. 1993, Vasco et al. 1994). We have adopted an alternative approach based upon the minimization of the l^p norm of the residual vector (Nolet 1987). The power p may be chosen such that model parameter estimates are approximately maximum likelihood estimates (Vasco et al. 1994). In our particular application the value of p is 1.25, derived from an analysis of our composite data set (Vasco and Johnson 1998). Defining

$$\mathbf{M} = [\ \mathbf{V}\ \ \mathbf{H}\ \ \mathbf{S}\ \ \mathbf{B}\ \ \mathbf{A}\ ], \quad (3)$$

and $\delta\mathbf{x} = [\delta\mathbf{v}\ \delta\mathbf{h}\ \delta\mathbf{s}\ \delta\mathbf{b}\ \delta\mathbf{a}]^T$ we may write the l^p residual norm minimization problem in a compact form,

$$min \sum_{i=1}^{M} |\sum_{j=1}^{N} M_{ij}\delta x_j - \delta T_i|^p \quad (4)$$

where N is the total number of parameters and M is the total number of constraints. An efficient algorithm for the general l^p residual norm inversion has been presented by *Scales et al.* [1988]. The technique is based upon repeatedly solving a weighted system of linear equations,

$$\mathbf{N}^{1/2}\mathbf{M}\delta\mathbf{x} = \mathbf{N}^{1/2}\delta\mathbf{T} \quad (5)$$

where the weights, contained in $\mathbf{N}^{1/2}$, are varied systematically. The weighting or scaling matrix $\mathbf{N}^{1/2}$ is diagonal and it's ith diagonal element is

$$N_i{}^{1/2} = |\sum_{j=1}^{N} M_{ij}\delta x_j - \delta T_i|^{p-2}. \quad (6)$$

The solution of equation (5), $\delta\mathbf{x}$, is used to compute the set of scaling factors ($N_i{}^{1/2}$) in equation (6), the equations are rescaled, and the weighted system of

equations (5) is solved again. The procedure is repeated for a number of steps until satisfactory convergence is achieved.

The weighted system of equations may be represented in a standard form if we define $\mathbf{G} = \mathbf{N}^{1/2}\mathbf{M}$ and $\delta\mathbf{d} = \mathbf{N}^{1/2}\delta\mathbf{T}$ then

$$\mathbf{G}\delta\mathbf{x} = \delta\mathbf{d}. \tag{7}$$

To solve this system of equations we employ the singular value decomposition (SVD) of $\mathbf{G}$, described next.

Inference and assessment based upon the SVD

The estimation of model parameter resolution and model parameter covariance follows from a singular value decomposition (SVD) of the matrix $\mathbf{G}$ in equation (7). The SVD is a representation of $\mathbf{G}$ as the product of three matrices

$$\mathbf{G} = \mathbf{U}\mathbf{\Lambda}\mathbf{V}^T \tag{8}$$

where $\mathbf{\Lambda}$ is a diagonal matrix of singular values (Menke, 1984; Golub and Van Loan, 1989). The matrices $\mathbf{U}$ and $\mathbf{V}$ are orthogonal, that is they satisfy $\mathbf{U}^T\mathbf{U} = \mathbf{I}$ and $\mathbf{V}^T\mathbf{V} = \mathbf{I}$. Equation (8) may be derived from an eigen-decomposition of the $L \times L$ ($L = M + N$) matrix

$$\mathbf{A} = \begin{pmatrix} \mathbf{0} & \mathbf{G} \\ \mathbf{G}^T & \mathbf{0} \end{pmatrix} \tag{9}$$

(Menke 1984, Berry 1992), resulting in the two systems of linear equations

$$\mathbf{G}\mathbf{v}_i = \lambda_i \mathbf{u}_i \tag{10}$$

$$\mathbf{G}^T\mathbf{u}_i = \lambda_i \mathbf{v}_i$$

which may be written

$$\mathbf{G}^T\mathbf{G}\mathbf{v}_i = \lambda^2{}_i \mathbf{v}_i \tag{11}$$

$$\mathbf{G}\mathbf{G}^T\mathbf{u}_i = \lambda^2{}_i \mathbf{u}_i,$$

where λ_i is the ith diagonal element of $\mathbf{\Lambda}$. In matrix form equation (10) is

$$\mathbf{G}\mathbf{V} = \mathbf{U}\mathbf{\Lambda} \tag{12}$$

or

$$\mathbf{G} = \mathbf{U}\mathbf{\Lambda}\mathbf{V}^T. \tag{13}$$

The least squares solution $\delta\hat{\mathbf{x}}$ of the regularized inverse problem, which may be written in terms of a truncation of the SVD, is used to construct the generalized inverse of $\mathbf{G}$ (denoted by $\mathbf{G}^\dagger$)

$$\mathbf{G}^\dagger = \mathbf{V}_p\mathbf{\Lambda}_p{}^{-1}\mathbf{U}_p{}^T \tag{14}$$

where the subscript p signifies that only the p largest singular values and their accompanying singular vectors are retained. The solution to equation (7) is then

$$\delta\hat{\mathbf{x}} = \mathbf{V}_p\mathbf{\Lambda}_p{}^{-1}\mathbf{U}_p{}^T\delta\mathbf{d}. \tag{15}$$

Model parameter resolution is a quantitative measure of averaging or blurring inherent in model parameter estimates (Menke, 1984; Parker, 1994) derived by assuming that a 'true' solution to equation (7), denoted by $\delta\mathbf{x}_t$, exists. Because $\delta\mathbf{x}_t$ satisfies equation (7), substituting $\mathbf{G}\delta\mathbf{x}_t$ for $\delta\mathbf{d}$ in equation (15) and making use of equation (7), results in

$$\delta\hat{\mathbf{x}} = \mathbf{G}^\dagger\mathbf{G}\delta\mathbf{x}_t = \mathbf{V}_p\mathbf{V}_p{}^T\delta\mathbf{x}_t = \mathbf{R}\delta\mathbf{x}_t. \tag{16}$$

The elements of a row of the resolution matrix $\mathbf{R} = \mathbf{G}^\dagger\mathbf{G}$ are averaging coefficients quantifying the contribution which all parameters make to the estimates. That is, the R_{ij} element of the resolution matrix represents the contribution of the j-th parameter to an estimate of the i-th parameter. For the generalized inverse based upon truncation, the averaging results from retaining only p singular values and vectors rather than utilizing the full spectrum.

The model covariance matrix contains measures of the uncertainties associated with the model parameters as well as the mapping of the uncertainty between parameters. In particular, the diagonal elements are the variances corresponding to the estimates. Assuming that the data are uncorrelated with uniform variance, $\sigma_d{}^2$, the model parameter covariance matrix is given by (Menke, 1984; Parker, 1994)

$$\mathbf{C}_m = \sigma_d{}^2\mathbf{G}^\dagger(\mathbf{G}^\dagger)^T = \sigma_d{}^2\mathbf{V}_p\mathbf{\Lambda}_p{}^{-2}\mathbf{V}_p{}^T. \tag{17}$$

Thus, under the stated assumptions, both the resolution and covariance matrices may be derived directly from the singular value decomposition of the matrix $\mathbf{G}$. We should note that there are alternatives to the SVD for computing resolution and covariance matrices, for example the LU decomposition approach of Vasco et al. (1993) which is based upon the approach of Tarantola (1987).

Partial SVD using Lanczos recursion

Overview. The SVD approach to model assessment is computationally intensive and only practical

for small to moderately sized inverse problems. For this reason the vast majority of tomographic models are not accompanied by formal estimates of model parameter resolution and uncertainty. Rather, approximate measures of spatial averaging and uncertainty, such as checkerboard tests and inversions of numerical noise, are presented. Recently there have been a number of publications (Scales 1989, Nolet and Snieder 1990, Berryman 1994, Zhang and McMechan 1995, Minkoff 1996, Vasco et al. 1998) advocating approximate model assessments based upon efficient iterative inversion techniques such as the LSQR algorithm (Paige and Saunders, 1982). The approximate techniques have the advantage of presenting the model assessment in terms of useful quantities such as the model parameter resolution and covariance matrices. However, as pointed out by Deal and Nolet (1996), and discussed at the end of this section, the numerical approximation methods produce lower bounds on model parameter resolution and should not be interpreted as strict SVD-based resolution estimates.

The most widely suggested numerical device for implementing an approximate model assessment is the Lanczos algorithm. This is a three term recursion, originally suggested by Lanczos (1950), with links to conjugate gradient methods (Cullum and Willoughby 1985) such as the LSQR algorithm. In outline, the Lanczos procedure transforms a given $L \times L$ matrix $\mathbf{A}$, such as in equation (9), to an $l \times l$ tridiagonal matrix $\mathbf{T}$ using an orthogonal transformation $\mathbf{Q}$:

$$\mathbf{T} = \mathbf{Q}^T \mathbf{A} \mathbf{Q} \tag{18}$$

where $\mathbf{Q}^T\mathbf{Q} = \mathbf{I}$ and the columns of $\mathbf{Q} = [\mathbf{q}_1, \mathbf{q}_2, ...\mathbf{q}_l]$ are known as Lanczos vectors (Lanczos, 1950; Cullum and Willoughby, 1985). For $L = l$ the eigenvalues of $\mathbf{T}$ are identical to those of $\mathbf{A}$ and the eigenvectors are simply found by matrix multiplication of the eigenvectors of $\mathbf{T}$ by the Lanczos vectors. Equation (18) and the orthogonality of $\mathbf{Q}$ implies that

$$\mathbf{A}\mathbf{Q} = \mathbf{Q}\mathbf{T}. \tag{19}$$

Because $\mathbf{T}$ is tridiagonal

$$\mathbf{T} = \begin{pmatrix} \alpha_1 & \beta_2 & & \dots & 0 \\ \beta_2 & \alpha_2 & \beta_3 & & \\ & \ddots & \ddots & \ddots & \\ & & & & \beta_l \\ 0 & & & \beta_l & \alpha_l \end{pmatrix} \tag{20}$$

equation (19) is equivalent to the system of l equations

$$\mathbf{A}\mathbf{q}_i = \beta_i \mathbf{q}_{i-1} + \alpha_i \mathbf{q}_i + \beta_{i+1}\mathbf{q}_{i+1} \quad i = 1, 2, ..., l \tag{21}$$

the recursion of Lanczos (1950), where $\mathbf{q}_0 = \mathbf{0}$ and the orthonormality of the Lanczos vectors $\mathbf{Q}$ is used to choose β_1. The sequence of equations (21) is started with an arbitrary non-zero vector $\mathbf{q}_1$ of unit length. The full Lanczos scheme consists of the steps:

For $\mathbf{q}_0 = \mathbf{0}$ and $\mathbf{s}_1$ arbitrary and $\beta_1 = ||\mathbf{s}_1||$, $i = 1, 2, ..., l$

$$\begin{aligned} \mathbf{q}_i &= \mathbf{s}_i/\beta_i \\ \mathbf{r}_i &= \mathbf{A}\mathbf{q}_i - \beta_i \mathbf{q}_{i-1} \\ \alpha_i &= \mathbf{r}_i{}^T \mathbf{q}_i \\ \mathbf{s}_{i+1} &= \mathbf{r}_i - \alpha_i \mathbf{q}_i \\ \beta_{i+1} &= ||\mathbf{s}_{i+1}|| \end{aligned} \tag{22}$$

upon completion of l steps we have the matrices $\mathbf{T}$ and $\mathbf{Q}$ from which the eigenvalues and eigenvectors of $\mathbf{A}$ may be estimated. When l equals the order of the matrix $\mathbf{A}$, L, the eigen-decomposition is identical to a conventional SVD of the matrix $\mathbf{G}$. Typically many fewer than L steps are actually needed for the convergence of eigenvalues and eigenvectors. A rough rule of thumb is that the first $l/2$ eigenvalues have converged to those which would be produced by a conventional SVD.

Proceeding from the Lanczos algorithm there are at least two ways to obtain the necessary quantities for resolution and covariance estimates. The complete approach begins with the composite matrix ($\mathbf{A}$) in equation (9) and requires more computation and storage. A more efficient technique is to work with the matrix $\mathbf{G}^T\mathbf{G}$ and directly calculate the coefficients of $\mathbf{V}_p$ and $\mathbf{\Lambda}_p$ needed in equations (16) and (17). In the following two sub-sections we describe both approaches.

Application to the matrix A. A decomposition similar to the SVD of $\mathbf{G}$, equation (13), follows from an eigen-decomposition of the real symmetric tridiagonal matrix $\mathbf{T}$

$$\mathbf{T} = \mathbf{W}\mathbf{\Lambda}\mathbf{W}^T \tag{23}$$

where $\mathbf{W}$ is an orthogonal matrix containing the eigenvectors of $\mathbf{T}$ as columns and $\mathbf{\Lambda}$ is a diagonal matrix containing the eigenvalues of $\mathbf{T}$. [Because $\mathbf{W}$ is orthogonal, it satisfies $\mathbf{W}\mathbf{W}^T = \mathbf{W}^T\mathbf{W} = \mathbf{I}$ (Golub and Van Loan 1989)] Substituting equation (23) in equation (18) and pre- and post- multiplying by $\mathbf{W}^T$ and $\mathbf{W}$ respectively we have

$$\mathbf{\Lambda} = \mathbf{W}^T\mathbf{Q}^T\mathbf{A}\mathbf{Q}\mathbf{W}$$

after making use of the orthogonality of $\mathbf{W}$. Defining $\mathbf{S} = \mathbf{QW}$ we have the diagonalization of $\mathbf{A}$

$$\mathbf{\Lambda} = \mathbf{S}^T\mathbf{AS}.$$

Note, from equation (9), that $\mathbf{A}$ is a partitioned matrix and write $\mathbf{S}$ (the matrix of eigenvectors of $\mathbf{A}$) in a partitioned form

$$\mathbf{S} = \begin{pmatrix} \mathbf{U} \\ \mathbf{V} \end{pmatrix}.$$

Thus, the upper half of each column of the matrix $\mathbf{S} = \mathbf{QW}$ contains the left singular vectors $\mathbf{u}_i$ while the lower half contains the right singular vectors $\mathbf{v}_i$ and $\mathbf{\Lambda}$ contains the singular values as its diagonal elements. Equations (10) through (12) may then be used to construct the singular value decomposition of $\mathbf{G}$ as given in equation (13) as well as the generalized inverse defined by equation (14).

Application to the matrix $\mathbf{G}^T\mathbf{G}$. If we are only interested in calculating elements of the resolution and covariance matrices we can reduce the amount of computation somewhat. Examining equations (16) and (17) we see that only the right singular vectors $\mathbf{V}$ and the singular values $\mathbf{\Lambda}$ are necessary in constructing the resolution matrix $\mathbf{R}$ and the covariance matrix $\mathbf{C}_m$. Therefore, rather than starting with the composite matrix $\mathbf{A}$ given by equation (9) we consider the real symmetric matrix $\mathbf{G}^T\mathbf{G}$ and its eigen-decomposition, as in equation (11). It is important to note that the potentially dense matrix $\mathbf{G}^T\mathbf{G}$ is never explicitly formed in the decomposition. Remember that for the Lanczos decomposition, as written in (22), we only require the matrix-vector multiply $\mathbf{t}_i = \mathbf{G}^T\mathbf{G}\mathbf{q}_i$. This is done in two steps, first forming $\mathbf{y}_i = \mathbf{G}\mathbf{q}_i$ and then $\mathbf{t}_i = \mathbf{G}^T\mathbf{y}_i$. Thus, we can retain the advantages associated with any sparsity of $\mathbf{G}$.

Instead of equation (18) we have the matrix equation

$$\mathbf{T} = \mathbf{Q}^T\mathbf{G}^T\mathbf{GQ} \tag{24}$$

where $\mathbf{T}$ is tridiagonal and $\mathbf{Q}$ is orthogonal as in (18). An eigen-decomposition of $\mathbf{T}$, as in equation (23), produces

$$\mathbf{\Lambda} = \mathbf{W}^T\mathbf{Q}^T\mathbf{G}^T\mathbf{GQW}$$

or

$$\mathbf{G}^T\mathbf{G} = \mathbf{V\Lambda V}^T \tag{25}$$

where $\mathbf{V} = \mathbf{QW}$. The matrix $\mathbf{V}$, or rather its first p columns are exactly what we need to compute the resolution and covariance estimates as in equations (16) and (17). In fact, this is the procedure we follow in our application to the whole Earth imaging problem.

To find a solution [which requires the left singular vectors $\mathbf{U}$, as indicated in equation (15)] we used the LSQR algorithm of Paige and Saunders (1982). This algorithm is routinely used in seismic tomography since its potential was highlighted by Nolet (1985, 1987) and Scales (1987). The LSQR algorithm or some modification of it has been used in a number of tomographic studies [see Iyer and Hirahara (1993) for an overview of seismic tomography]. Particular applications to whole mantle tomography have been numerous since the study by Inoue et al. (1990). We have found the algorithm to have many desirable properties, including rapid convergence, numerical stability, and efficiency (Pulliam et al. 1993, Vasco et al. 1994, Vasco et al. 1995, Vasco and Johnson 1998). LSQR follows from an application of the Lanczos recursion to the symmetric system

$$\mathbf{A} = \begin{pmatrix} \mathbf{I} & \mathbf{G} \\ \mathbf{G}^T & -\eta^2\mathbf{I} \end{pmatrix}$$

(Paige and Saunders 1982) which is the coefficient matrix for damped least squares (η is the damping parameter). We shall not go into the mechanics of the LSQR algorithm but refer interested readers to the more detailed references given above.

Notes on the numerical implementation and convergence. There are several aspects of the algorithm of equation (22) which bear on its numerical implementation. First, the Lanczos vectors tend to lose orthogonality as the iteration proceeds. There are several remedies for this and the one we use is selective re-orthogonalization (Simon 1984, Sehmi 1989, Berry 1992, Vasco et al. 1998). Specifically, a recursive measure of orthogonality is computed at each iteration and re-orthogonalization is enforced only when necessary. Another important factor is the iterative nature of the approach. As the number of iterations approaches the rank of the matrix $\mathbf{G}$, the singular value and vector estimates given above approach the singular values and vectors of $\mathbf{G}$. However, for l steps of the algorithm (22), where l is much less than the rank of $\mathbf{G}$, only the largest singular value estimates will approximate the true singular values. As a rough rule of thumb, the first $l/2$ singular value estimates will have converged. The other values are associated with linear combinations of singular vectors, the subspace spanned by vectors with nearby singular values. Even though elements of the later part of the spectrum have not converged to any particular sin-

gular value-singular vector pair they are still useful in providing a low rank approximation to $\mathbf{G}$ (Xu and Kailath 1994, Simon and Zha 1998) and may be used in resolution and covariance calculations. Specifically, the Lanczos decomposition of $\mathbf{G}^T\mathbf{G}$, as in equation (25), may be used in equations (16) and (17) producing expressions for the Lanczos resolution and covariance matrices (Berryman 1994, Zhang and McMechan 1995).

As noted by Deal and Nolet (1996), the number of orthogonal vectors produced by the Lanczos algorithm can, in some cases, not adequately span the range of model space, producing resolution estimates which are significantly different from SVD resolution measures. For example, if we have completed l steps of the Lanczos algorithm and have a set of l orthonormal vectors $\mathbf{v}_i$, the column vectors of $\mathbf{V}$, the diagonal elements of the resolution matrix are given by

$$R_{ii} = \sum_{i=1}^{L} (\mathbf{v}_i)_i^{\,2} \geq \sum_{i=1}^{l} (\mathbf{v}_i)_i^{\,2}. \qquad (26)$$

Thus, for $l \leq L$ the Lanczos resolution estimates are lower bounds on the diagonal elements of the SVD resolution matrix. The difficulty described by Deal and Nolet (1996) is problem dependent, a function of the spectrum of singular values, and is found to occur when the number of orthogonal Lanczos vectors is several orders of magnitude smaller than the number of model parameters. As the spectrum flattens, the singular values become closer in value, and the sub-space spanned by the associated singular vectors becomes degenerate. Geometrically, the singular vectors have almost the same length, as measured by the singular values. Therefore, any linear combination of these vectors may be used to represent the sub-space they span. The Lanczos algorithm converges to some sub-set of these vectors and it is this subset that represents the entire sub-space. For singular values which are closely spaced, a nearly flat region of the spectrum, the sub-set will be an adequate representation and the resolution and covariance estimates will approach those of the SVD. However, we must adequately sample the spectrum, particularly elements from its tail. Obtaining enough singular values to sufficiently estimate resolution and covariance requires a substantial number of iterations beyond those required to converge to a solution. In the results presented below 5000 iterations were executed, 50 times the number of iterations used to produce the tomographic model. Because of the potential differences in resolution (and covariance) estimates computed by Lanczos iteration and the SVD, we feel it is important not to confuse the two measures. To distinguish our resolution and covariance estimates from the conventional SVD based quantities we label our estimates Lanczos resolution and Lanczos covariance, respectively.

DATA ANALYSIS

Data reduction and summary residual formation

Our data are primarily derived from the International Seismological Centre (ISC), consisting of travel time observations spanning the years 1964-1987. The raw data have been extensively re-processed as described in Vasco et al. (1994, 1995) and Vasco and Johnson (1998). In outline, the ISC events are relocated and the individual arrival times are culled and re-associated. The relocations and re-associations are with respect to the $ak135$ P and S velocity model (Kennett et al. 1995). Both P and S phases were used in the relocation procedure as described in Vasco et al. (1994), Vasco et al. (1995), and Vasco and Johnson (1998). The relocation process served as a culling process and events with less than 50 arrivals were not considered, eliminating over half of the ISC events. Our relocation and re-association procedure is similar to the reprocessing of Engdahl et al. (1998). Our culling was somewhat more stringent than that of Engdahl et al. (1998) and depth phases were not used to constrain event depth. We felt that, without a regional model which includes the influence of the overlying crust and upper mantle, inclusion of depth phases (which travel extensively in these regions) could potentially introduce additional bias in the relocation procedure.

Of the 19 phases we considered, 10 were deemed more reliable and least contaminated by other phases. We extracted 2,920,035 raw P, 730,979 raw S, 34,824 raw PP, 16,990 raw PcP, 15,494 raw SS, 4566 raw ScS, 49,965 raw $PKPab$, 77,894 raw $PKPbc$, 299,721 raw $PKPdf$, and 9170 raw $SKSac$ in total. To better constrain the mantle discontinuities at 410 and 660 km we included two sets of differential phases ($SS - S_{410}S$, $SS - S_{660}S$) derived from long period waveforms (Shearer 1993). The raw observations were corrected for the ellipticity of the Earth (Vasco and Johnson 1998). In addition, the surface reflected PP and SS were corrected for the topography at the bounce point. After re-association a travel time residual was calculated relative to the $ak135$ model. In

order to reduce the dependence of our results on the one-dimensional background velocity we removed the residual medians as a function of epicentral distance.

The re-processed ISC data set contains considerable redundancy. For example, there is a dominance of P observations from European and North American stations. To reduce the inhomogeneity in data coverage and to improve the signal to noise ratio we formed summary or composite residuals. Essentially this is a binning procedure in which residuals from nearby sources to a collection of nearby stations are averaged together. Our implementation entails dividing the upper 150 km into 3 layers, each 50 km thick, and sub-dividing each layer into a grid of equal area cells (2° by 2° at the equator). We take the median of all residuals of a particular phase with the same source cell and station cell. Only summary data not influenced by crossing (interfering) phases are used in the inversion as described by Vasco and Johnson (1998). In total there are 462,421 P, 199,193 S, 18,781 PP, 9429 PcP, 9421 SS, 3269 ScS, 13,297 $PKPab$, 14,443 $PKPbc$, 82,328 $PKPdf$, 6073 $SKSac$, and 1629 $SS-S_dS$ summary and differential phases.

To reduce the sensitivity of core phases to near source velocity variations, difference times are constructed. That is, for all phases traversing the inner or outer core we do not use the arrival time directly in the inversion. Rather, for a given event, the arrival time of the P observed at the most distant station is subtracted from the arrival time of the core phase. In forming such difference times we are attempting to reduce the effect of source mislocation and near surface velocity structure on our model parameter estimates. The difference times are 'backprojected' along the difference raypaths. That is, the sensitivity coefficients are given by the long offset P raypath minus the core raypath, with each raypath weighted by the inverse of the squared velocity along the raypaths. Thus, we account for the difference in the paths traveled by the two phases. Because we also include the long offset mantle P data in the inversion as an additional explicit constraint this approach is for the most part equivalent to our previous inversion (Vasco and Johnson 1998). However, any significant biases in the core residuals due to near source structure should be somewhat reduced by the differencing because they should also appear in the long offset P.

Two added benefits of summary data are that the number of rays which we must trace and the resulting system of equations which we must solve are significantly reduced. Such considerations are important because the raytracing consumes a sizable amount of computer time. Furthermore, though the Lanczos recursion is quite efficient it requires a substantial amount of computer memory to store the non-zero elements of $\mathbf{A}$ in core memory. The ability to place this matrix in memory provides a critical speed-up as may be seen in the Lanczos recursion given by algorithm (22). The matrix-vector multiply in this scheme is the most computationally burdensome step. Executing the vector-matrix multiply entirely in memory requires an order of magnitude less time than does accessing $\mathbf{A}$ from disk. Still, the computation of 5,000 Lanczos value-vectors pairs, about 1/20 of the entire spectrum (96,300 possible singular values), took approximately 6 weeks on a work station with 1 Gbyte of core memory. As we shall see, the computation may be done on a parallel processor with substantial speedup. On a 64 processor Cray T3E-900 at the National Energy Research Computing Center we computed 9,000 Lanczos vectors and values in just under 2 hours.

Regularization, weighting, and inversion

As discussed in the introduction, the sampling of the Earth by recorded seismic energy is quite variable. This inhomogeneity in raypath coverage can introduce numerical instability into algorithms for determining Earth structure. It is now standard practice to introduce some form of regularization or penalty constraints in order to stabilize the inversion. For the details of this methodology we refer the reader to books on inverse theory (Menke 1984, Parker 1994). Briefly, we augment the system of equations (7) with additional conditions constraining the Earth model. These additional equations follow either directly from the minimization of a penalized misfit functional or indirectly from the solution of a constrained inverse problem via the method of LaGrange multipliers (Parker 1994). Two common forms of regularization penalize model roughness and model norm as described in Menke (1984).

The truncation of singular vectors used in constructing an Earth model, as in equation (15), is a form of regularization related to a norm penalty or minimum norm constraint (Parker 1994). That is, when only p singular vectors and values are used to calculate $\delta\hat{\mathbf{x}}$ we are neglecting components in the model space associated with singular values less than λ_p. Hence, a norm constraint is inherent in our Lanczos inversion algorithm. A method related to trun-

cation is damping or filtering, where a scalar value η is used to avoid unwanted amplification of noise or numerical instability (Pratt and Chapman 1992). Specifically, equation (15) is replaced by

$$\delta\hat{\mathbf{x}} = \mathbf{V}_p\mathbf{\Lambda}_p{}^{-1}\mathbf{D}\mathbf{U}_p{}^T\delta\mathbf{d}. \tag{27}$$

where $\mathbf{D}$ is a diagonal matrix whose elements are given by

$$D_{ii} = \frac{\lambda_i{}^2}{\lambda_i{}^2 + \eta^2}. \tag{28}$$

This is the form of regularization which we shall use in our inversion, in addition to the truncation at p vectors. Note that the resolution and covariance matrices are also suitably modified to account for the damping (Pratt and Chapman 1992). The resolution matrix is given by

$$\mathbf{R} = \mathbf{V}_p\mathbf{D}\mathbf{V}_p{}^T$$

and the covariance matrix by

$$\mathbf{C}_m = \sigma_d{}^2\mathbf{V}_p(\mathbf{\Lambda}_p{}^{-1}\mathbf{D})^2\mathbf{V}_p{}^T.$$

The inversion relies on two cycles of iterations: Four outer iterations for the l_p norm minimization and inner iterations of varying length (1, 15, 30, 100) for the LSQR algorithm. At the completion of each outer iteration the data are reweighted before the next set of inner iterations. The Lanczos resolution and covariance are estimated using the weights output from the third set of iterations, before the final outer cycle. Thus, we are incorporating the re-weightings prior to the final linear inversion (final LSQR cycle). Using these weights and the coefficient matrix $\mathbf{G}$ we then compute our 5,000 Lanczos values and vectors.

RESULTS

We now present the results of the Lanczos-based inversion and assessment. Though there are Lanczos resolution and covariance estimates for all 96,300 model parameters (P/S velocity variations, boundary deflections, inner core anisotropy, hypo-central parameters, and station corrections) in this section we shall focus on P and S velocity parameters and CMB boundary topography. In particular, only estimates of velocity heterogeneity (including inner core anisotropy) and core mantle boundary topography will be shown. The other parameter estimates did not differ substantially from those of Vasco and Johnson (1998) and will not be discussed here.

Before we interpret our results the issue of convergence of the Lanczos algorithm must be addressed. Specifically, do the Lanczos resolution and covariance measures adequately approximate the SVD resolution and covariance? Because it is not feasible to actually perform a numerical SVD we cannot directly compare the Lanczos resolution/covariance estimates to the SVD resolution/covariance estimates. However, as shown in Figure 1, we can examine the convergence of the resolution estimates as a function of the number of Lanczos vectors. In Figure 1 the ratio of the successive sums of the diagonal elements of the Lanczos resolution matrix, the trace of the resolution matrix, are plotted as a function of the number of Lanczos vectors used to construct the estimate. For less than about 3,000 Lanczos vectors there is a significant change in the Lanczos resolution diagonal sum as additional Lanczos vectors are added. The ratio of successive diagonal sums approaches 1 as more Lanczos vectors are included. By 5,000 Lanczos vectors the ratio is 0.9 and the change is 1.2 % from the previous ratio. Therefore, it appears that the diagonal of the Lanczos resolution matrix has converged to a large extent and further iteration will not significantly affect the results. However, as a check of our results, we shall compare the estimates presented below with previous formal estimates of resolution and covariance for mantle travel time tomography (Vasco et al. 1993) as well as with checkerboard inversions conducted for the whole Earth tomographic problem (Vasco and Johnson 1998). Finally, in the section Discussion and Conclusions we present results from a more extensive computation of Lanczos vectors and values. A total of 9,000 Lanczos vectors and values are used to construct estimates of model parameter resolution. A comparison with these more extensive calculations is evidence for the convergence of our estimates.

The spectrum of singular values is shown in Figure 2. There is a steep drop in spectral amplitude for the first 500 or so singular values. The spectrum tends to flatten out at around 2,000 singular values and it is likely that this reflects the behavior of the actual SVD spectrum. However, at around 3,000 singular vectors the spectrum declines more rapidly, a consequence of incomplete convergence to the spectral estimates. As mentioned above, these remaining spectral values are associated with linear combinations of singular vectors spanning nearly degenerate sub-spaces. The spectrum as a whole is a component of a valid low rank matrix approximation based upon the Lanc-

zos algorithm (Simon and Zha 1998). As such, we may use the spectrum in Figure 2 to choose a cutoff p of singular vectors to include in the inversion and Lanczos resolution and covariance calculations. We chose a cutoff of 1/1000 of the peak spectral amplitude in our calculations, retaining the first 4983 singular vectors. Based upon this cutoff the Lanczos resolution and covariance matrices are computed as in equations (16) and (17), respectively. We have normalized our estimates such that the rows are approximately uni-modular (Menke 1984, p. 73). That is, a random selection of 22 rows, associated with one cell from each layer, of the resolution matrix were derived and summed. A scaling factor was derived such that, when scaled, the elements in each row summed to 1. It is well known that there is a trade-off between model parameter resolution and model parameter covariance (Parker 1994). In our approach this trade-off may be parameterized by both the singular value cutoff and the degree of damping. In fact, we pick the cutoff based upon this trade-off. First we fix the damping at 1/1000 of the peak singular value. Then, for a sequence of singular value cutoffs, we calculated resolution and covariance estimates. Our cutoff was chosen such that the resolution and uncertainty lie within acceptable limits.

Lanczos resolution

The Lanczos model parameter resolution for portions of the mantle, the outer core, and the inner core are shown in Figure 3. Here the diagonal elements of the resolution matrix are shown for a large number of layers in our model. In each cell the associated Lanczos resolution estimate is plotted in a gray tone, darker tones signifying higher resolution. We treat these Lanczos estimates as lower bounds on the formal SVD-based resolution. The Lanczos resolution varies significantly as a function of position in the Earth. Overall, Lanczos resolution is highest in well sampled cells (see Vasco and Johnson 1998). The Lanczos resolution shares the same general features as the checkerboard inversion in Vasco and Johnson (1998): well resolved cells in the mantle beneath many continental regions, moderate resolution of outer core anomalies, and poor resolution of inner core velocity heterogeneity.

It is informative to compare our results with a previous resolution calculation based upon an LU decomposition of the matrix $\mathbf{G}^{\dagger}\mathbf{G}$ (Vasco et al. 1993). In that study only P data were used to constrain mantle compressional velocity heterogeneity. Furthermore, to keep the level of computation manageable, source and receiver corrections were not included directly in the inversion and assessment. Vasco et al. (1993) also included model smoothness as a regularization term in the inversion and assessment. In spite of these differences in methodology, the large scale pattern of the Lanczos resolution is similar to the resolution estimates of Vasco et al. (1993). This suggests that inclusion of the additional phases, while critical for determining CMB and core structure, does not substantially improve the overall resolution of mantle structure. There are approximately an order of magnitude more P observations than any other compressional phase and these data tend to dominate mantle resolution. The well resolved regions of Vasco et al. (1993) are somewhat broader than what is presented in Figure 3, the influence of the smoothing regularization incorporated into their inversion. As a final note, we emphasize that the comparison only considers the diagonal elements of the resolution matrix. There may be, in fact there are likely to be, notable changes in the off-diagonal elements for particular cells when additional phases are used. Due to space limitations we shall not examine the changes in off-diagonal elements in this paper.

In the uppermost mantle, Lanczos resolution is greatest in the major subduction zones encircling the Pacific and beneath the continents of the northern hemisphere. The co-location of seismic sources and seismographic stations in the Pacific subduction zones and tectonically active continental regions is primarily responsible for the well resolved circum-Pacific velocity heterogeneity. The mantle beneath oceanic ridges, another seismically active province, is moderately to poorly resolved. Lack of a significant number of stations in the world's ocean basins results in generally poor Lanczos resolution beneath the Pacific, Atlantic, and Indian ocean basins. Similarly, the majority of seismographic stations are in the northern hemisphere and correspondingly the resolution in the southern hemisphere is poor for the most part with exceptions under Australia, southern Africa, and western South America. The pattern of well resolved cells beneath the continents of the northern hemisphere and in a broad cicum-Pacific swath continues downward to mid and lower mantle depths (Figure 3). However, in the lowermost mantle, just above the core-mantle boundary (CMB), the Lanczos resolution decreases. Such a decrease in resolution was also observed in the LU decomposition calculations of Vasco et al. (1993) and in the checkerboard resolution esti-

mates of Vasco and Johnson (1998). It is most likely due to raypath geometry, the mantle P waves bottom in this layer and only core reflected and core transmitted phases pass completely through.

Our Lanczos resolution of mantle shear velocity shares many attributes with the resolution of compressional velocities. In general, the Lanczos resolution is lower for shear heterogeneity in the mantle. This reflects the fact that there are many fewer S observations than P data. To some degree the S Lanczos resolution may be influenced by the incomplete convergence of the algorithm but this is difficult to quantify. Previous comparisons of P and S checkerboard resolution estimates (Vasco et al. 1994) support the lower level of S Lanczos resolution seen here. The poor Lanczos resolution of S estimates in the lowest mantle (2670 km-CMB) may be the result of 2 factors. First, our cutoff of S observations at 82° to avoid interference with SKS. Secondly, the constraints on S heterogeneity provided by ScS and $SKSac$ tradeoff with CMB topography and outer core heterogeneity. Additional data is required to better constrain S heterogeneity just above the CMB.

The Lanczos resolution in the outer core retains many of the features seen in the overlying mantle. This is not surprising because the dominant propagation paths are extensions of the waves through the mantle. For example, the Lanczos resolution associated with cells in the outer core beneath the ocean basins is very poor. Taking the outer core as a whole the resolution is approximately half that of the overlying mantle. As observed by Vasco and Johnson (1998), velocity estimates in the outer core are associated with greater vertical averaging than are mantle estimates. Due to the ray geometry and the nature of propagation in the outer core, depth resolution is less than in the mantle and estimates are averages over 1 to 3 layers. We shall have more to say about this below when we examine particular rows of the resolution matrix associated with blocks in the outer core. The resolution is best in the mid to lower outer core because this region is constrained by the more numerous $PKPab$ and $PKPbc$ which bottom in the outer core in addition to $PKPdf$ which also propagates through the inner core. The poor resolution of outermost core structure has been noted previously (Garnero and Helmberger 1995).

The Lanczos resolution of velocity heterogeneity in the inner core is uniformly poor (Figure 3). This is consistent with checkerboard tests described by Vasco and Johnson (1998). There are several reasons for our inability to constrain velocity heterogeneity in the inner core. We have included terms for inner core anisotropy in the inversion which can trade-off with isotropic velocity heterogeneity. The cell volumes becomes increasingly smaller as the Earth's center is approached. In the inner core the block volumes are quite small and it is difficult to constrain single block anomalies. The inner core has a small total volume and lies deep within the Earth's interior. Using seismic energy generated near the Earth's surface it is difficult to resolve velocity variations in the inner core.

The cross section at 175° E summarizes the Lanczos resolution of the Earth's compressional velocity structure (Figure 4). Clearly, large volumes within the Earth are poorly resolved by seismic observations and our knowledge of Earth structure varies strongly with location. Parts of the mantle are quite well resolved at the scale of a single cell, particularly in the northern hemisphere. The velocity variations in the outer core are moderately well resolved while heterogeneity in the inner core is not well determined.

In order gain a deeper understanding of our resolution of outer core heterogeneity we examine three rows of the resolution matrix associated with cells there. For example, in Figure (5a) we display constant depth and constant longitude sections through the averaging kernel of cell 8607. This block is located beneath the Solomon Islands in the depth range 3671-4071 km, almost midway into the outer core. From the constant depth section there appears to be little lateral averaging between cell 8607 and adjacent blocks. The constant longitude section through the block indicates averaging with cells in the overlying and underlying layers. This accounts for the moderate resolution 0.5 associated with this volume element. Cell 8319, located beneath Hawaii in the same depth range (3671-4071 km), is poorly resolved (Lanczos resolution: 0.06) due to insufficient sampling (Figure 5b). The constant depth section displays clear lateral averaging within the layer. The constant longitude section does not display the depth averaging but this appears to be due to it's orientation. From the depth section it appears that the averaging kernel is elongated transverse to the longitudinal section. Volume element (Voxel) 5562 is situated at the base of the outer core below the East Pacific ridge. The Lanczos resolution for this cell is 0.2 and from the depth section in Figure 5c lateral averaging is apparent within the layer. From the constant longitude section there does not appear to be significant tradeoff with inner core velocity estimates. This was verified

by examining various other longitude sections, and it appears that the radial averaging extends to overlying cells to the north and east of block 5562 rather than down into the inner core. From the three averaging kernels we see that in areas of moderate resolution averaging between adjacent layers dominates. Similar vertical smearing between adjacent layers in the outer core was seen in checkerboard tests from the whole Earth inversion of Vasco and Johnson (1998). In poorly resolved regions it appears that lateral averaging may also be significant.

Lanczos covariance

The Lanczos covariance estimates are computed as in equation (17), using the decomposition of (25). In constructing the defining linear system of equations (7) we scale each equation by the inverse of the standard deviation of each datum. The procedure is described in Pulliam et al. (1993) and Vasco et al. (1993). Thus, the equations are normalized to have unit standard deviations and equation (17) may be used directly. The standard deviations are derived from the summary residuals which are binned by increments of epicentral distance. The standard deviation is calculated for each bin and for each phase and this value is used to scale the row. This weighting is re-calculated with each re-weighting in the outer iteration of the robust inversion algorithm. The singular value cutoff is identical to that used in the resolution calculations, 1/1000 th of the peak spectral amplitude. The resulting standard deviations, the square root of the diagonal elements of the covariance matrix, are shown in Figure 6. Note that the gray scale is reversed, high standard deviations are indicated by lighter tones. The results for the mantle are quite close to the values found by Vasco et al. (1993) using an LU decomposition.

Overall, the standard deviation is lowest in the well resolved portions of the mantle, of the order of 0.1 %. In cells sampled by few rays and which are poorly resolved the standard deviation is large, between 0.5 and 15 %. This pattern, poorly constrained blocks associated with large uncertainties, is what one would expect. However, inversions of random deviates, which are often used to estimate model parameter uncertainty, do not generally produce the greatest deviations in poorly sampled voxels (For example, the inversion of random deviates in Vasco and Johnson (1998) has small standard deviations below the mid-Pacific in the depth range 35-200 km, a region of high uncertainty). In the upper mantle, blocks below the continents of the northern hemisphere and in subduction zone source regions have the smallest standard deviation. There is a broadening of this pattern with depth into the mantle. Estimates of mantle velocity structure below the Pacific basin have large uncertainties (0.5 % or greater) well into the lower mantle. Estimate for cells in the southern-most portion of the mantle are also more uncertain due to poor coverage.

Shear velocity estimates have a much higher level of uncertainty than do estimates of compressional velocity. This is due to higher data uncertainties, as all shear phases are secondary arrivals and are accompanied by signal generated noise. In addition, there are many fewer observed shear phase arrival times resulting in fewer constraints overall. The variation in shear velocity standard deviation in the mantle is much like that of the compressional velocity. However, in the lowest mantle the standard deviation is much larger for S than for P. This is due to the cutoff of S arrival times for stations beyond 82° from the source. Thus, only ScS and $SKSac$ phases constrain the lowest mantle and these phases have even larger uncertainties than does S. In the mantle shear estimates some cells in regions with very few raypaths are mapped to zero, perhaps due to incomplete convergence of the Lanczos algorithm.

In the outer core the standard error generally decreases with depth, reflecting the denser sampling by $PKPab$ and $PKPbc$ phases in the mid to lower outer core. In well resolved regions the standard deviation ranges from 0.1 to 0.2 % while in poorly resolved cells it exceeds 0.5 %. The large scale pattern resembles that seen in the mid-mantle: smaller standard deviations beneath the continents in the northern hemisphere and arc-trench source regions, higher standard deviations in the southern hemisphere and beneath the ocean basins. Near the top of the outer core more than half of the volume of the layers are poorly constrained with large associated uncertainties. Further into the outer core the standard error distribution becomes more uniform. At the base of the outer core estimates in the southern hemisphere have the largest uncertainties.

In the inner core there is a systematic increase in model parameter uncertainty with depth. Uncertainties are smallest in the depth range ICB-5371 km beneath Asia and the northwestern Pacific Ocean basin. The standard deviation is consistently larger in the southern hemisphere and beneath the south-central Pacific. Velocity estimates in the final 2 layers are

generally of the order of 0.4 % or greater. The reasons for the large uncertainties below 5671 km are the small volume occupied by the cells at this radius and the tradeoff with velocity anisotropy.

Global Earth structure

We can now interpret our estimates of Earth structure in the context of the model assessment given above. To facilitate the determination of the well constrained portions of the model we shall only display those anomalies which are significant. That is, all anomalies which are below the estimated P standard deviation will not be plotted. Such a presentation reduces the chance of interpreting poorly constrained velocity variations. We used the P standard error because there is the possibility of incomplete convergence influencing the S covariance estimates.

The velocity heterogeneity we estimate is shown in Figure 7. Many of the features in our mantle model agree with previous mantle P inversions (Inoue et al. 1990) and S inversions (Li and Romanowicz 1996, Masters et al. 1996). The shallow mantle (35-200 km) is dominated by high velocities associated with the continental cratons and a circum-Pacific low velocity ring. Intermittent high velocity anomalies correlating with known subduction zones are seen most strongly in the S model. Oceanic ridge anomalies lie in poorly resolved regions of the model and are not shown. The correlation between of P and S velocity anomalies in this layer is quite strong, though there are differences in amplitude. High velocities under the cratons continues until around 400 km when the amplitude decreases and in some cases the anomalies disappear altogether. High velocities associated with subduction zones are seen beneath east Asia and South America in both the P and S models. By 660 km depth high velocities which might be related to subduction zones are strong (1-2 %) as both P and S anomalies. Again, the P and S patterns of heterogeneity are similar though there is more small scale variation in S which may be due to the lower signal-to-noise ratio of S arrival times. In many areas the circum-Pacific fast anomalies extend to depths of 900 km or more. For example, high velocity P and S perturbations are seen beneath India and Indonesia in the depth range 1270-1470 km and beneath Central and South America. Such high velocity anomalies have been observed by Inoue et al. (1990), Vasco et al. (1995), Robertson and Woodhouse (1995), van der Hilst (1997), Vasco and Johnson (1998). The velocity variations beneath southern Eurasia may be related to earlier subduction in the region. It is worth pointing out that the P anomalies are well resolved, as indicated in Figure 3, at the scale of our inversion. In the lowest mantle (2670 km-CMB) there are high velocities below eastern Asia and India as well as under North and Central America. Significant averaging due to the ray geometry in this layer limits the lateral resolution of velocity heterogeneity (Figure 3).

The depth variations of the core mantle boundary are also shown in Figure 7. In this figure blue colors denote a deeper boundary while red signifies a shallower interface. The broad variation agrees with the recent PcP inversion results of Rodgers and Wahr (1993) and the P and PcP inversion of Obayashi and Fukao (1997), a deeper boundary at low latitudes and a shallower boundary for much of the northern higher latitudes. The CMB topography must be interpreted with care because it is not possible to distinguish between heterogeneity in a thin layer about the boundary and undulations of the boundary itself using arrival times (Rodgers and Wahr 1994). Furthermore, there are indications that a thin very low velocity zone may exists just above the CMB (Garnero and Helmberger 1996, Williams and Garnero 1996).

In the shallow outer core it is difficult to constrain velocity variations because so few rays bottom there. In our data set only 6073 $SKSac$ bottom in the shallow outer core. It is not until the third layer (3671-4071 km) of the outer core that a significant proportion of cells contain anomalies exceeding their standard deviations. At the base of the outer core there appears to be a systematic variation in velocity with latitude. Specifically, velocities near the equatorial plane appear faster than those in the polar regions. The same variation was noted by Vasco and Johnson (1998) and remained even when $PKPdf$ arrival times were not used in the inversion, suggesting that the pattern in not induced by inner core structure. There have been other studies noting variations in residuals bottoming in the outer core as a function of latitude (Gudmundsson 1989, Roudil and Souriau 1993) as well as investigations indicating weak heterogeneity in the outer core (Souriau and Poupinet 1990, 1991, Tanaka and Hamaguchi 1993). Such heterogeneity may be induced by external density anomalies or boundary forcing (Wahr and de Vries 1989). However, more work is necessary to ensure that the pattern is not the mapping of overlying heterogeneity, such as near the core-mantle boundary or near the Earth's surface, into the outer core.

In our model inner core heterogeneity is only con-

strained between the inner core boundary (ICB) and 5671 km. The decreasing volume of our cells with radius, coupled with the inclusion of parameters for inner core anisotropy, tend to reduce the resolution of inner core velocity heterogeneity. Even the top 2 layers in the inner core are, for the most part, poorly determined. The longitudinal variation seen in the overlying outer core is not evident in the solid inner core. In general it is difficult to discern any overall pattern such as the hemispherical variation observed by others (Tanaka and Hamaguchi 1997).

The variation in direction and magnitude of inner core anisotropy is shown in Figure 8. This figure depicts both the magnitude and direction of fastest velocity. The peak anisotropy magnitude is 2.6 % and the fast directions are dominantly polar. As noted by Vasco et al. (1998) the direction of peak velocity is sensitive to ray geometry and trades off with lateral variations in isotropic heterogeneity. Note the decrease in anisotropy magnitude with depth in the inner core. This is due to the interaction with the model norm constraint and the poor constraints provided by the data below 5671 km depth.

DISCUSSION AND CONCLUSIONS

Because of the heterogeneous distribution of earthquakes and seismographic stations our knowledge of the Earth's internal structure is a strong function of position. In spite of our use of an extensive number of phases, 12 in all, there are still large variations in ray coverage between cells in our model. In the face of such variability it is essential to conduct as complete a model assessment as possible. The results presented here indicate that it is feasible to compute measures of resolution and covariance. The time required for the construction, approximately 6 weeks of computation, is of the order of that required for a complete suite of checkerboard tests and inversions of random deviates. For example, in Vasco and Johnson (1998) a checkerboard inversion was required for each layer (22) for P, for all mantle layers for S (12), and for the core mantle boundary. In addition, 20 inversions of synthetic random deviates were needed to reliably estimate the model noise level. Each of these tests requires of the order of a day of computation for a total of 54 days of calculation. As mentioned in the introduction, there are a number of disadvantages associated with the synthetic inversions: dependence on particular checkerboard pattern, inverting synthetic random deviations is strongly influenced by regularization resulting in incorrect uncertainty estimates. While the Lanczos resolution is approximate and requires a sufficient number of iterations for convergence, it is a conservative measure and does not suffer from the drawbacks of synthetic tests. The Lanczos approach also provides additional useful information. For example, the averaging kernel for any parameter is computed quite simply. Also, the SVD spectrum is useful in regularizing the inverse problem based upon a cutoff of singular values.

Due to the iterative nature of our Lanczos procedure there is the possibility of inadequate convergence to formal resolution and covariance measures. That is, computational considerations limit the number of iterations which we can execute. For example, in the preceding analysis we were limited to 5,000 Lanczos values and vectors. In order to examine if 5,000 Lanczos iterations are enough for estimating resolution and covariance for our whole Earth imaging problem we conducted additional iterations. Specifically, using a block Lanczos algorithm (Sehmi 1989, Berry 1992) on a massively parallel Cray T3E-900 at the Department of Energy's National Energy Research Computing Center (NERSC) a total of 9,000 Lanczos vectors and values were calculated. The parallel algorithm scaled quite well with the number of processors and we were able to compute the necessary Lanczos vectors and values in under 2 hours on 64 processors. This should be contrasted with the 6 weeks required to compute 5,000 vectors/values on a scalar workstation. The resulting singular value estimates are shown in Figure 9 (filled squares) along with the previous estimates from Figure 2 (crosses). For approximately the first 3,000 singular values there is excellent agreement before the rapid decrease for estimates associated with 5,000 Lanczos vector-value pairs. As noted earlier, the singular value estimates in the latter part of the spectrum are associated with linear combinations of singular vectors which define nearly degenerate sub-spaces. The important question is: Have we adequately sampled the spectrum. Stated differently, do we have a dense enough sample of the range of spectral amplitudes? One way to answer this question is to use the additional Lanczos values to compute model parameter resolution. In Figure 10 we compare diagonal elements of the resolution matrix for layers in the mantle and outer core using 5,000 and 9,000 Lanczos vectors. The geographical and radial variations in model parameter resolution are quite similar overall. There are slight differences in amplitude but the small variations will not change

our interpretation in any significant way.

There is evidence that significant intermediate and small scale heterogeneity exists in the mantle (Gudmundsson et al. 1990, Passier and Snieder 1995, Hedlin et al. 1997). A model which only allows for large scale variations in velocity will map such structure as artifacts (Trampert and Snieder 1996). Thus, it is desirable to obtain higher resolution images of the Earth and there are efforts to that end (Fukao et al. 1992, van der Hilst et al. 1997). These studies find anomalies seen in larger scale inversions (Inoue et al. 1990, Vasco et al. 1995, Vasco and Johnson 1998). In particular, fairly continuous high velocity anomalies beneath southern Eurasia and beneath the Americas. However, when estimating small scale structural variations we must be mindful of the tradeoff between resolution and uncertainty (Backus and Gilbert 1967, 1968). The construction of resolution and uncertainty, as outlined here, are necessary when interpreting such detailed structural models. In fact our results indicate that, at least for the scale of our cells (6° by 6° at the equator), the fast P anomalies are well resolved. Additional work is necessary to determine if it is possible to resolve the structure in significantly more detail.

The approach described in this paper is very general and may be applied to the joint inversion of arrival times and waveforms. Such joints inversions, particularly those incorporating body and surface waves, should better constrain upper mantle structure. Improved modeling and inversion algorithms such as Li and Romanowicz (1996) should help in that regard, providing sensitivity kernels with information on spatial averaging.

Acknowledgments. This work was supported by a Laboratory Directed Research and Development grant, U. S. Department of Energy under Contract No. DE-AC03-76SF00098. Support was also provided by the Defense Special Weapons Agency under grant DSWA-01-97-1-0026. All computations were carried out at the Center for Computational Seismology and the National Energy Research Computing (NERSC) Center, LBL.

References

Backus, G. E., 1965. Possible forms of seismic anisotropy of the uppermost mantle under oceans, *J. Geophys. Res.*, **70**, 3429-3439.

Backus, G. and Gilbert, J. F., 1967. Numerical applications of a formalism for geophysical inverse problems, *Geophys. J. R. Astron. Soc.*, **13**, 247-276.

Backus, G. and Gilbert, J. F., 1968. The resolving power of gross earth data, *Geophys. J. R. Astron. Soc.*, **16**, 169-205.

Berry, M., 1992. Large scale singular value computations, *Internat. J. Supercomp. Appl.*, **6**, 13-49.

Berryman, J. G., 1994. Tomographic resolution without singular value decomposition, in Mathematical Methods in Geophysical Imaging II, *Proc. of SPIE, 2301*, pp. 2-13, edited by Hassanzadeh, S., SPIE, Bellingham.

Bunge, H.-P. and M. A. Richards, 1996. The origin of large scale structure in mantle convection: effects of plate motions and viscosity stratification, *Geophys. Res. Lett.*, **23**, 2987-2990.

Clayton, R. W., and R. P. Comer, 1983. A tomographic analysis of mantle heterogeneities from body wave travel times, *Eos Trans. AGU*, **64**, 776.

Creager, K. C., 1992. Anisotropy of the inner core from differential travel times of the phases PKP and $PKIKP$, *Nature*, **356**, 309-314.

Creager, K. C., and T. H. Jordan, 1986. Aspherical structure of the core-mantle boundary from PKP travel times, *Geophys. Res. Lett.*, **13**, 1497-1500.

Cullum, J. K., Willoughby, R. A., 1985. *Lanczos Algorithms for Large Symmetric Eigenvalue Computations, Vol. I Theory*, Birkhauser.

Davies, G. F., 1990. Mantle plumes, mantle stirring and hotspot chemistry, *Earth and Planet. Sci. Lett.*, **99**, 94-109.

Deal, M. M., and Nolet, G., 1996. Comment on "Estimation of resolution and covariance for large matrix inversions" by Zhang and McMechan, *Geophys. J. Int.*, **127**, 245-250.

Dziewonski, A.M., B.H Hager, and R.J. O'Connell, 1977. Large-scale heterogeneities in the lower mantle, *J. Geophys. Res.*, **82**, 239-255.

Engdahl, E. R., R. D. van der Hilst, and R. P. Buland, 1998. Global teleseismic earthquake relocation with improved travel times and procedures for depth determination, *Bull. Seism. Soc. Am.*, **88**, 722-743.

Fukao, Y., M. Obayashi, H. Inoue, and M. Nenbai, 1992. Subducting slabs stagnant in the transition zone, *J. Geophys. Res.*, **99**, 2809-2822.

Garnero, E. J., and Helmberger, D. V., 1995. On seismic resolution of lateral heterogeneity in the Earth's outermost core, *Phys. Earth and Planet. Int.*, **88**, 117-130.

Garnero, E. J., and Helmberger, D. V., 1996. Seismic detection of a thin laterally varying boundary layer at the base of the mantle beneath the central-Pacific, *Geo-*

phys. Res. Lett., **23**, 977-980.

Glatzmaier, G. A., and P. H. Roberts, 1995. A three-dimensional convective dynamo solution with rotating and finitely conducting inner core and mantle, *Phys. Earth Plan. Int.*, **91**, 63-75.

Glatzmaier, G. A., and P. H. Roberts, 1996. Rotation and magnetism of Earth's inner core, *Science*, **274**, 1887-1891.

Golub, G. H., and Van Loan, C. F., 1989. *Matrix Computations*, John Hopkins University Press.

Grand, S., 1990. A possible station bias in travel time measurements reported to the ISC, *Geophys. Res. Lett.*, **17**, 17-20.

Gudmundsson, O., 1989. Some problems in global tomography: Modeling the core-mantle boundary and statistical analysis of travel-time data, *Ph.D. thesis, Calif. Inst. of Technol.*, Pasadena.

Gudmundsson, O., J. H. Davies, and R. W. Clayton, 1990. Stochastic analysis of global travel time data: Mantle heterogeneity and random errors in the ISC data, *Geophys. J. Int.*, **102**, 25-44.

Gurnis, M., and G. Davies, 1986. Mixing in numerical models of mantle convection incorporating plate kinematics, *J. Geophys. Res.*, **91**, 6375-6395.

Gurnis, M., and S. Zhong, 1991. Generation of long-wavelength heterogeneity in the mantle by dynamic interaction between plates and convection, *Geophys. Res. Lett.*, **18**, 581-584.

Hedlin, M. A., Shearer, P. M., and Earle, P. S., 1997. Waveform stacks of PKP precursors: Evidence for small-scale heterogeneity throughout the mantle, *Nature*, ,.

Inoue, H., Y. Fukao, K. Tanabe, and Y. Ogata, 1990. Whole mantle *P*-wave travel time tomography, *Phys. Earth Planet. Inter.*, **59**, 294-328.

Iyer, H. M., and K. Hirahara, 1993. *Seismic Tomography: Theory and Practice*, Chapman and Hall, London.

Jeffreys, H., 1932. An alternative to the rejection of observations, *Proc. R. Soc. London*, **187**, 78-87.

Kennett, B. L. N., E. R. Engdahl, and R. Buland, 1995. Constraints on seismic velocities in the Earth from traveltimes, *Geophys. J. Int.*, **122**, 108-124.

Lanczos, C., 1950. An iterative method for the solution of the eigenvalue problem of linear differential and integral operators, *J. Res. Nat. Bur. Stand.*, **45** , 255-282.

Leveque, J.-J., L. Rivera, and G. Wittlinger, 1993. On the use of the checker-board test to assess the resolution of tomographic inversions, *Geophys. J. Int.*, **115**, 313-318.

Li, X. D., and B. Romanowicz, 1996. Global mantle shear velocity model developed using nonlinear asymptotic coupling theory, *J. Geophys. Res.*, **101**, 22,245-22,272.

Lux, R. A., G. F. Davies, and J. H. Thomas, 1979. Moving lithospheric plates and mantle convection, *Geophys. J. R. Astron. Soc.*, **57**, 209-228.

Masters, G., S. Johnson, G. Laske, and H. Bolton, 1996. A shear-velocity model of the mantle, *Philos. Trans. R. Soc. London Ser. A*, **354**, 1385-1411.

Menke, W., 1984. *Geophysical Data Analysis: Discrete Inverse Theory*, Academic Press, Orlando.

Minkoff, S. E., 1996. A computationally feasible approximate resolution matrix for seismic inverse problems, *Geophys. J. Int.*, **126**, 345-359.

Morelli, A., and A. M. Dziewonski, 1987. Topography of the core-mantle boundary and lateral homogeneity of the liquid core, *Nature*, **325**, 678-683.

Morelli, A., A. M. Dziewonski, and J. H. Woodhouse, 1986. Anisotropy of the inner core inferred from *PKIKP* travel times, *Geophys. Res. Lett.*, **13**, 1545-1548.

Nolet, G., 1985. Solving or resolving inadequate and noisy tomographic systems *J. Comput. Phys.*, **61** , 463-482.

Nolet, G., 1987. Seismic wave propagation and seismic tomography, in *Seismic Tomography*, edited by G. Nolet, pp. 1-23, D. Reidel, Norwell, Mass.

Nolet, G., and Snieder, R., 1990. Solving large linear inverse problems by projection, *Geophys. J. Int.*, **103** , 565-568.

Nolet, G., S. P. Grand, and B. L. N. Kennett, 1994. Seismic heterogeneity in the upper mantle, *J. Geophys. Res.*, **99** , 23753-23766.

Obayashi, M., and Y. Fukao, 1997. *P* and *PcP* travel time tomography for the core-mantle boundary *J. Geophys. Res.*, **102**, 17,825-17,841.

Paige, C. C., and Saunders, M. A., 1982. LSQR: An algorithm for sparse linear equations and sparse linear systems, *ACM Trans. Math. Software*, **8** , 195-209.

Parker, R. L., 1994. *Geophysical Inverse Theory*, Princeton University Press, Princeton, New Jersey.

Passier, M. L., and R. K. Snieder, 1995. On the presence of intermediate-scale heterogeneity in the upper mantle, *Geophys. J. Int.*, **123**, 817-837.

Poupinet, G., R. Pillet, and A. Souriau, 1983. Possible heterogeneity of the Earth's core deduced from PKIKP travel times, *Nature*, **305**, 204-206.

Pratt, R. G., and Chapman, C. H., 1992. Traveltime tomography in anisotropic media-II. Application, *Geophys. J. Int.*, **109** , 20-37.

Pulliam, R. J., D. W. Vasco, and L. R. Johnson, 1993. Tomographic inversions for mantle *P* wave velocity structure based on the minimization of l^2 and l^1 norms of International Seismological Centre travel time residuals, *J. Geophys. Res.*, **98**, 699-734.

Robertson, G. S., and J. H. Woodhouse, 1995. Evidence for proportionality of *P* and *S* heterogeneity in the lower mantle, *Geophys. J. Int.*, **123**, 85-116.

Rodgers, A., and J. Wahr, 1993. Inference of core-mantle boundary topography from ISC *PcP* and *PKP* traveltimes, *Geophys. J. Int.*, **115**, 991-1011.

Rodgers, A., and J. Wahr, 1994. The trade-off between volumetric and topographic structure for seismic traveltimes: 660 km topography and mantle structure, *Geo-*

phys. J. Int., **117**, 19-32.

Romanowicz, B., 1991. Seismic tomography of the Earth's mantle, *Annu. Rev. Earth Planet. Sci.*, **19**, 77-99.

Roudil, P., and Souriau, A., 1993. Liquid core structure and PKP station anomalies derived from $PKP(BC)$ propagation times, *Phys. Earth Planet. Inter.*, **77**, 225-236.

Scales, J. A., 1987. Tomographic inversion via the conjugate gradient method, *Geophysics*, **52** , 179-185.

Scales, J. A., 1989. On the use of conjugate gradient to calculate the eigenvalues and singular values of large, sparse matrices, *Geophys. J.*, **97** , 179-183.

Scales, J. A., Gersztenkorn, A., and Treitel, S., 1988. Fast l_p solution of large, sparse, linear systems, application to seismic travel time tomography: *J. Comp. Phys.*, **75**, 314-333.

Sehmi, N. S., 1989. *Large Order Structural Eigenanalysis Techniques*, John Wiley and Sons.

Sengupta, M. K., and M. N. Toksoz, 1976. Three-dimensional model of seismic velocity variation in the Earth's mantle, *Geophys. Res. Lett.*, **3**, 84-86.

Shearer, P. M., 1994. Constraints on inner core anisotropy from PKP(DF) travel times, *J. Geophys. Res.*, **99**, 19647-19659.

Shearer, P. M., 1993. Global mapping of upper mantle reflectors from long-period SS precursors, *Geophys. J. Int.*, **115**, 878-904.

Shearer, P. M., and T. G. Masters, 1992. Global mapping of topography on the 660-km discontinuity, *Nature*, **355**, 791-796.

Shearer, P. M., K. M. Toy, and J. A. Orcutt, 1988. Axisymmetric Earth models and inner-core anisotropy, *Nature*, **333**, 228-232.

Simon, H. D., 1984. The Lanczos algorithm with partial reorthogonalization, *Math. Comp.*, **42**, 115-142.

Simon, H. D., and H. Zha, 1998. Low rank matrix approximation using the Lanczos bidiagonalization process, *pre-print.*

Snieder, R., J. Beckers, and F. Neele, 1991. The effect of small-scale structure on normal mode frequencies and global inversions, *J. Geophys. Res.*, **96**, 501-515.

Song, X. D., and D. V. Helmberger, 1993. Anisotropy of Earth's inner core, *Geophys. Res. Lett.*, **20**, 2591-2594.

Song, X. D., and P. G. Richards, 1996. Seismological evidence for differential rotation of the Earth's inner core, *Nature*, **382**, 221-224.

Souriau, A., and G. Poupinet, 1990. A latitudinal pattern in the structure of the outermost liquid core, revealed by the travel times of $SKKS - SKS$ seismic phases, *Geophys. Res. Lett.*, **17**, 2005-2007.

Souriau, A., and G. Poupinet, 1991. A study of the outermost liquid core using differential travel times of the SKS, $SKKS$, and $S3KS$ phases, *Phys. Earth Planet. Inter.*, **68**, 183-199.

Tackley, P. J., D. J. Stevenson, G. A. Glatzmaier, and G. Schubert, 1993. Effects of an endothermic phase transition at 670 km depth on a spherical model of convection in Earth's mantle, *Nature*, **361**, 699-704.

Tanaka, S., and H. Hamaguchi, 1993. Degree one heterogeneity at the top of the Earth's core, revealed by $SmKS$ travel times, in *Dynamics of Earth's Deep Interior and Earth Rotation*, Geophys. Monogr. Ser., vol. 72, edited by J.-L. Le Mouël, D. E. Smylie, and T. Herring, pp. 127-134, AGU, Washington, D.C.

Tanaka, S., and H. Hamaguchi, 1997. Degree one heterogeneity and hemispherical variation of anisotropy in the inner core from $PKP(BC) - PKP(DF)$ times, *J. Geophys. Res.*, **102**, 2925-2938.

Tanimoto, T., 1986. The Backus-Gilbert approach to the 3D structure in the upper mantle. II. SH and SV velocity, *Geophys. J. R. Astron. Soc.*, **84**, 49-69.

Tarantola, A., 1987. *Inverse Problem Theory: Methods for Fitting and Model Parameter Estimation*, Elsvier.

Trampert, J., and R. Snieder, 1996. Model estimations biased by truncated expansions: Possible artifacts in seismic tomography, *Science*, **271**, 1257-1260.

Tromp, J., 1993. Support for anisotropy of the Earth's inner core from free oscillations, *Nature*, **366**, 678-681.

van der Hilst, R. D., S. Widiyantoro, and E. R. Engdahl, 1997. Evidence for deep mantle circulation from global tomography, *Nature*, **386**, 578-584.

Vasco, D. W., and Johnson, L. R., 1998. Whole Earth structure estimated from seismic arrival times, *J. Geophys. Res.*, **103**, 2633-2671.

Vasco, D. W., Pulliam, R. J., and Johnson, L. R., 1993. Formal inversion of ISC arrival times for mantle P-velocity structure, *Geophys. J. Int.*, **113**, 586-606.

Vasco, D. W., R. J. Pulliam, L. R. Johnson, and P. S. Earle, 1994. Robust inversion of IASP91 travel time residuals for mantle P and S velocity structure, earthquake mislocations, and station corrections, *J. Geophys. Res.*, **99**, 13727-13755.

Vasco, D. W., Pulliam, R. J., and Johnson, L. R., 1995. Lateral variations in mantle velocity structure and discontinuities determined from P, PP, S, SS, and SS-SdS travel time residuals, *J. Geophys. Res.*, **100**, 24,037-24,059.

Vasco, D. W., Peterson, J. E., and Majer, E. L., 1998. Resolving seismic anisotropy: Sparse matrix methods for geophysical inverse problems, *Geophysics*, **63**, 970-983.

Vinnik, L., B. Romanowicz, and L. Breger, 1994. Anisotropy in the center of the inner core, *Geophys. Res. Lett.*, **21**, 1671-1674.

Wahr, J., and D. de Vries, 1989. The possibility of lateral structure inside the core and its implications for nutation and Earth tide observations, *Geophys. J. Int.*, **99**, 511-519.

Williams, Q., and E. J. Garnero, 1996. Seismic evidence for partial melt at the base of the Earth's mantle, *Science*, **273**, 1528-1530.

Woodhouse, J. H., D. Giardini, and X.-D. Li, 1986. Ev-

idence for inner core anisotropy from free oscillations, *Geophys. Res. Lett.*, **13**, 1549-1552.

Xu, G., and T. Kailath, 1994. Fast estimation of principal eigenspace using Lanczos algorithm, *SIAM J. Matrix Anal. Appl.*, **15**, 974-994.

Zhang, J., and McMechan, G. A., 1995. Estimation of resolution and covariance for large matrix inversions, *Geophys. J. Int.*, **121**, 409-426.

D. W. Vasco, Center for Computational Seismology, Earth Sciences Division, Berkeley Laboratory, 1 Cyclotron Road, Berkeley, CA 94720. (e-mail: dwvasco@lbl.gov)

1998

[1]Also at Berkeley Seismological Laboratory, University of California, Berkeley.

This preprint was prepared with AGU's LaTeX macros v4. File lanczos formatted December 10, 1998.

Figure 1. Ratio of sum of the diagonal elements (trace) of the Lanczos resolution matrix as a function of the number of Lanczos vectors included in the calculation. Each point signifies the current diagonal sum divided by the previous diagonal sum.

Figure 2. Singular values derived from the Lanczos recursion. A total of 5,000 Lanczos vectors/values are used in constructing the spectrum.

Figure 3. Lanczos resolution estimates for the mantle, outer core, and inner core. For the mantle Lanczos resolution for both compressional and shear velocities are shown.

Figure 4. Lanczos resolution estimates for a cross-section through the Earth at 175° E.

Figure 5. (a) Lanczos averaging kernel for volume element 8607, located near the center of the outer core. Both a constant depth section and a constant longitude section are shown. (b) Same as above for cell 8319. (c) Same as above for cell 5562.

Figure 6. Lanczos standard deviations for the mantle, outer core, and inner core. In the mantle standard deviations are shown for compressional velocities only. The standard deviations are in percent variation with respect to the radial average.

Figure 7. Compressional and shear velocity estimates for the mantle as well as compressional velocity estimates for the outer core and inner core. The lateral variations in velocity are displayed in percent deviation from the background *ak*135 velocity model.

Figure 8. Variations in direction and magnitude of inner core anisotropy. The length of the arrow denotes the anisotropy magnitude. The angle with respect to the vertical signifies the angle between the Earth's rotation axis and the direction of maximum velocity.

Figure 9. A comparison of singular values derived from the Lanczos recursion based upon a total of 5,000 Lanczos vectors/values (crosses) with estimates based upon 9,000 Lanczos vector-value pairs (filled squares).

Figure 10. The diagonal elements of the resolution matrix for 3 mantle and 3 outer-core depth ranges. The panels on the left were computed using 5,000 Lanczos vectors while those on the right incorporate a more extensive set of 9,000 Lanczos vectors.

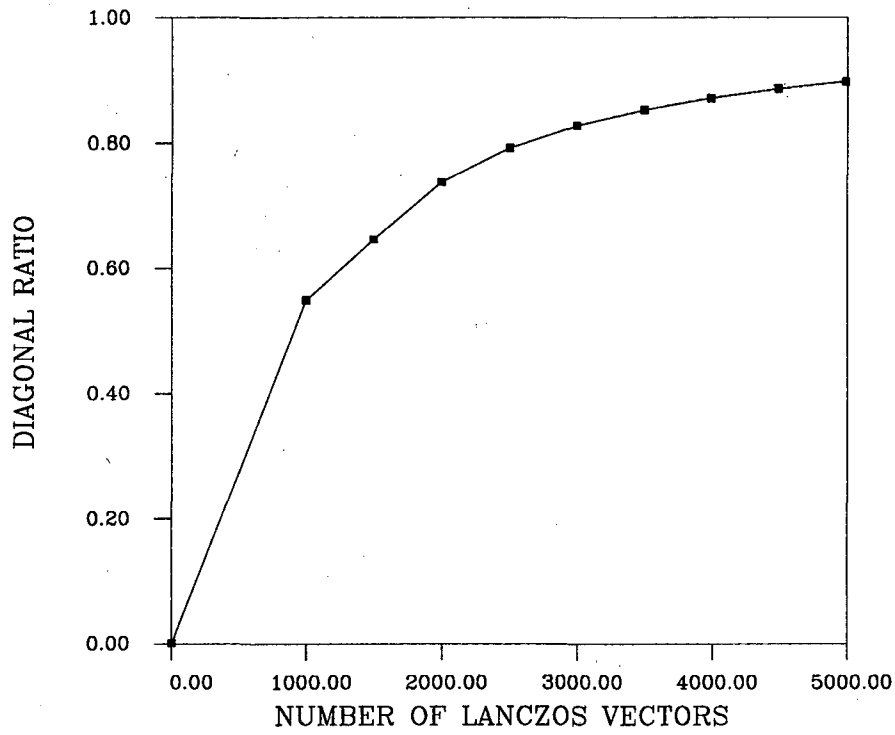
1.00
0.80
0.60
0.40
0.20
0.00
DIAGONAL RATIO
0.00
1000.00
2000.00
3000.00
4000.00
5000.00
NUMBER OF LANCZOS VECTORS

Figure 1

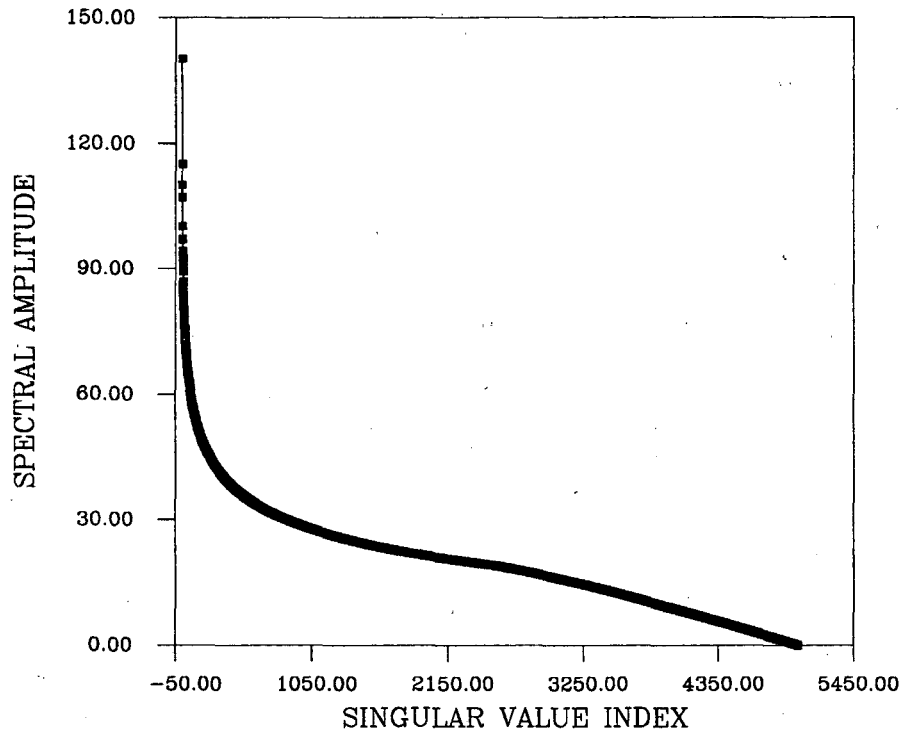
150.00
120.00
90.00
60.00
30.00
0.00
SPECTRAL AMPLITUDE
-50.00
1050.00
2150.00
3250.00
4350.00
5450.00
SINGULAR VALUE INDEX

Figure 2

Mantle - Compressional

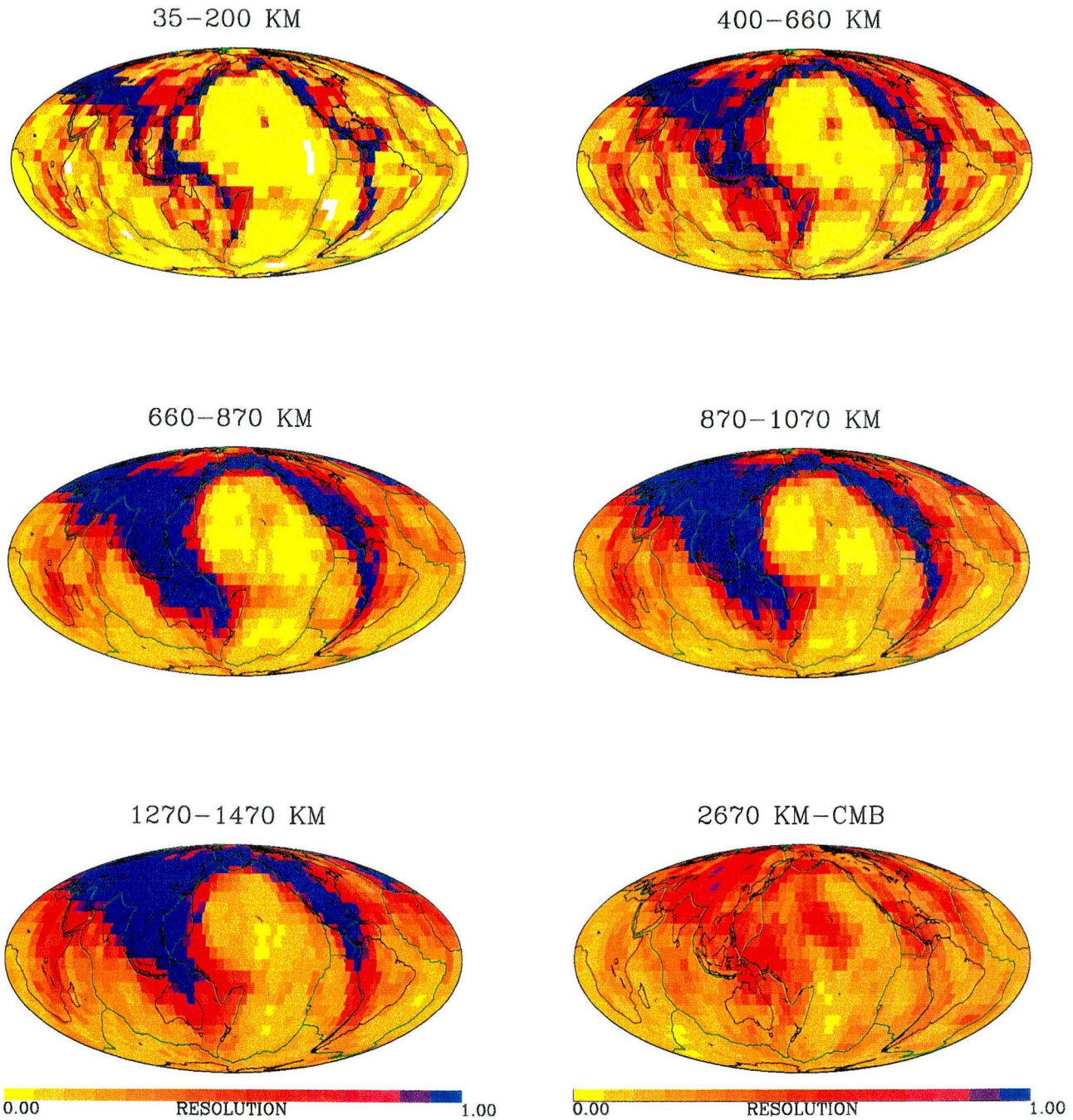

Figure 3.a

Mantle - Shear

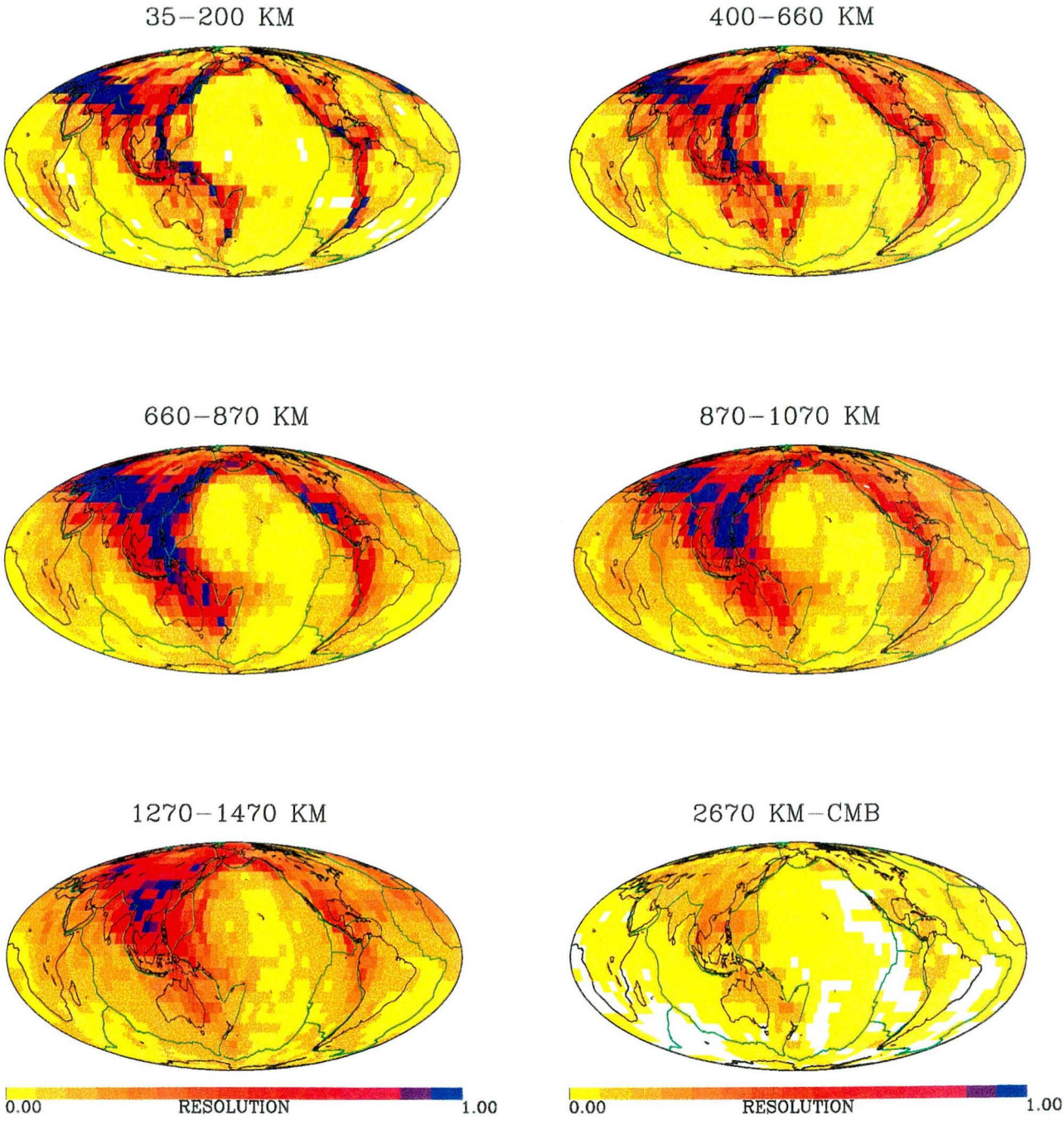

Figure 3.b

Outer Core - Compressional

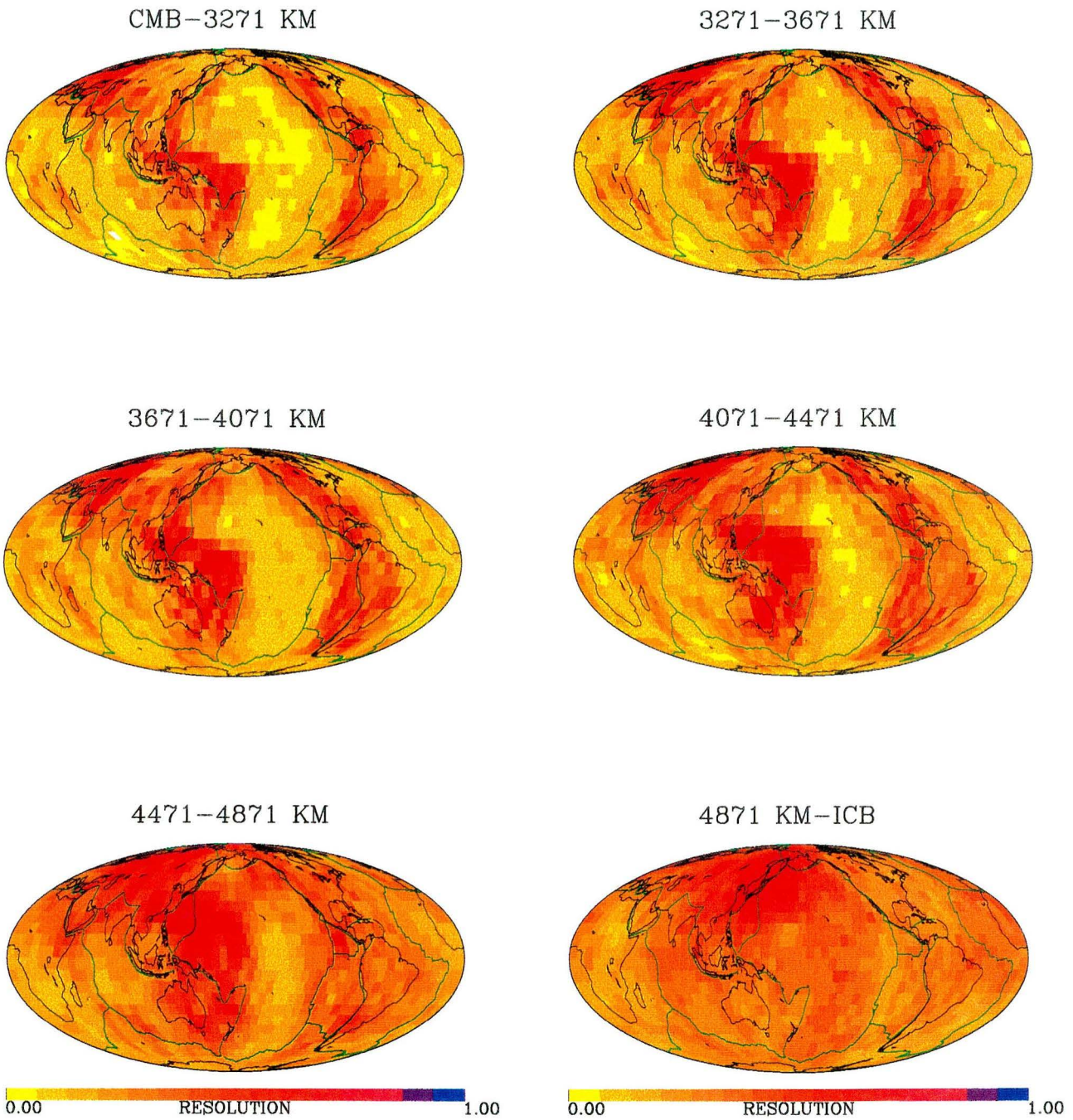

Figure 3.c

Inner Core - Compressional

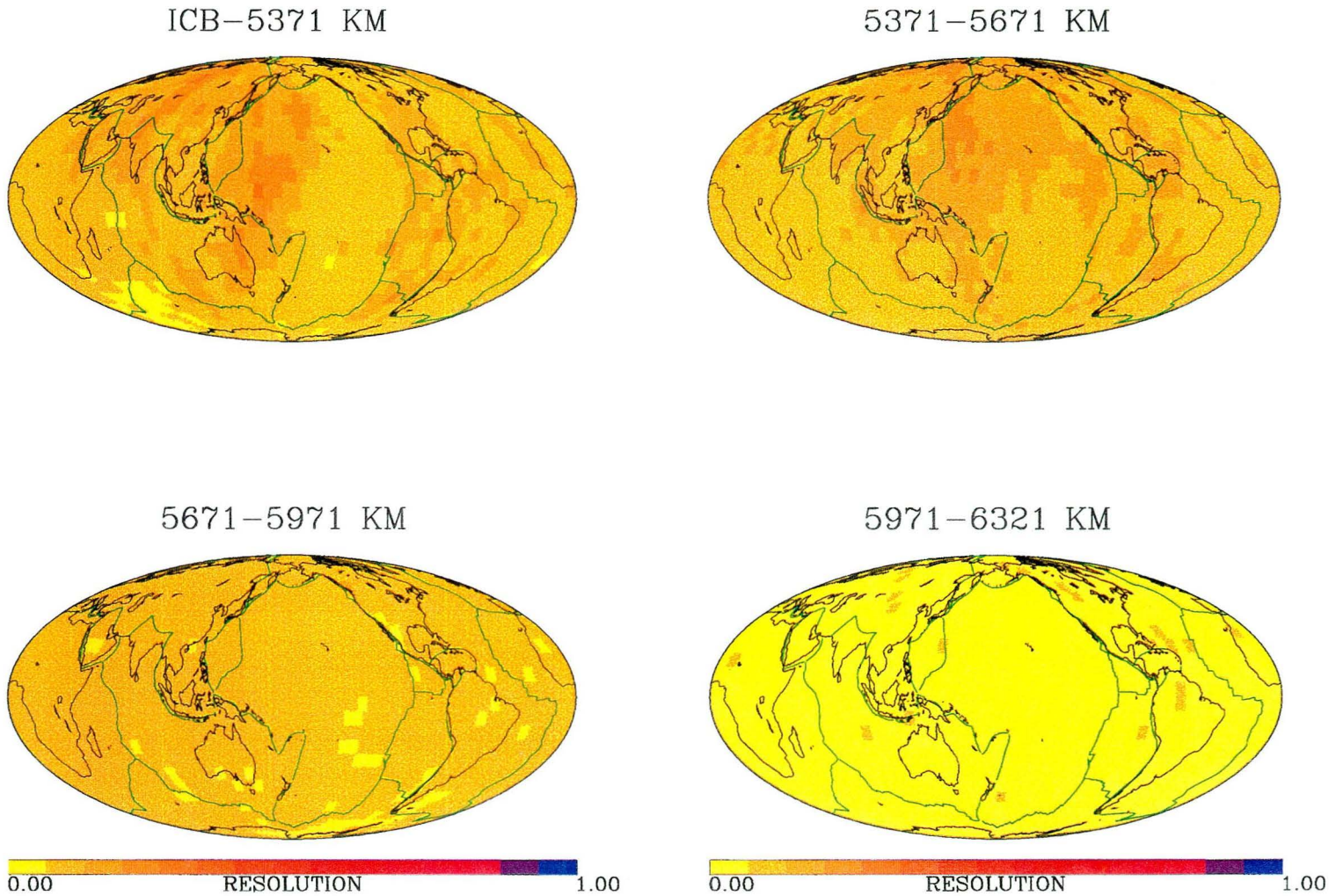

Figure 3.d

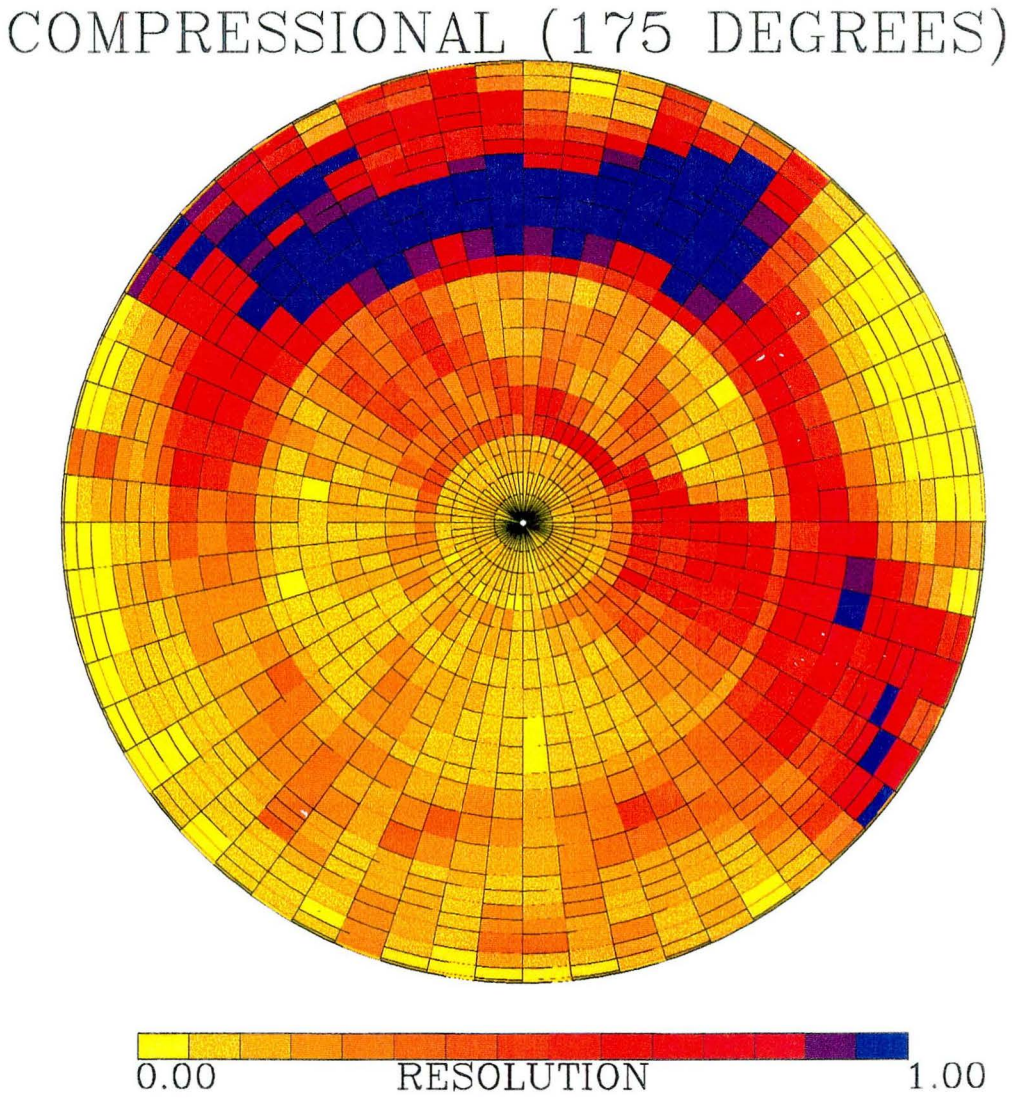

Figure 4

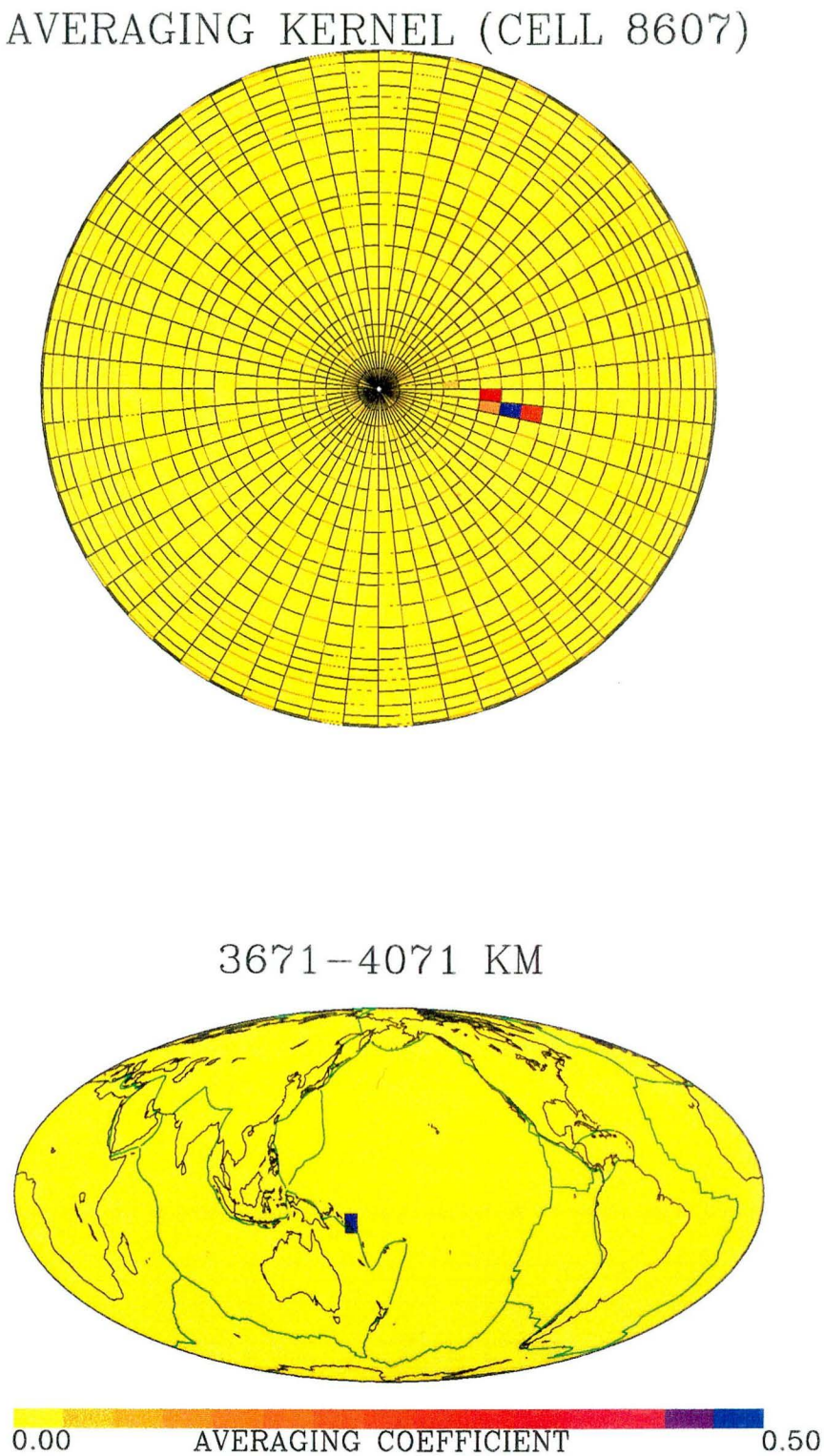
AVERAGING KERNEL (CELL 8607)
3671–4071 KM
0.00
AVERAGING COEFFICIENT
0.50

Figure 5.a

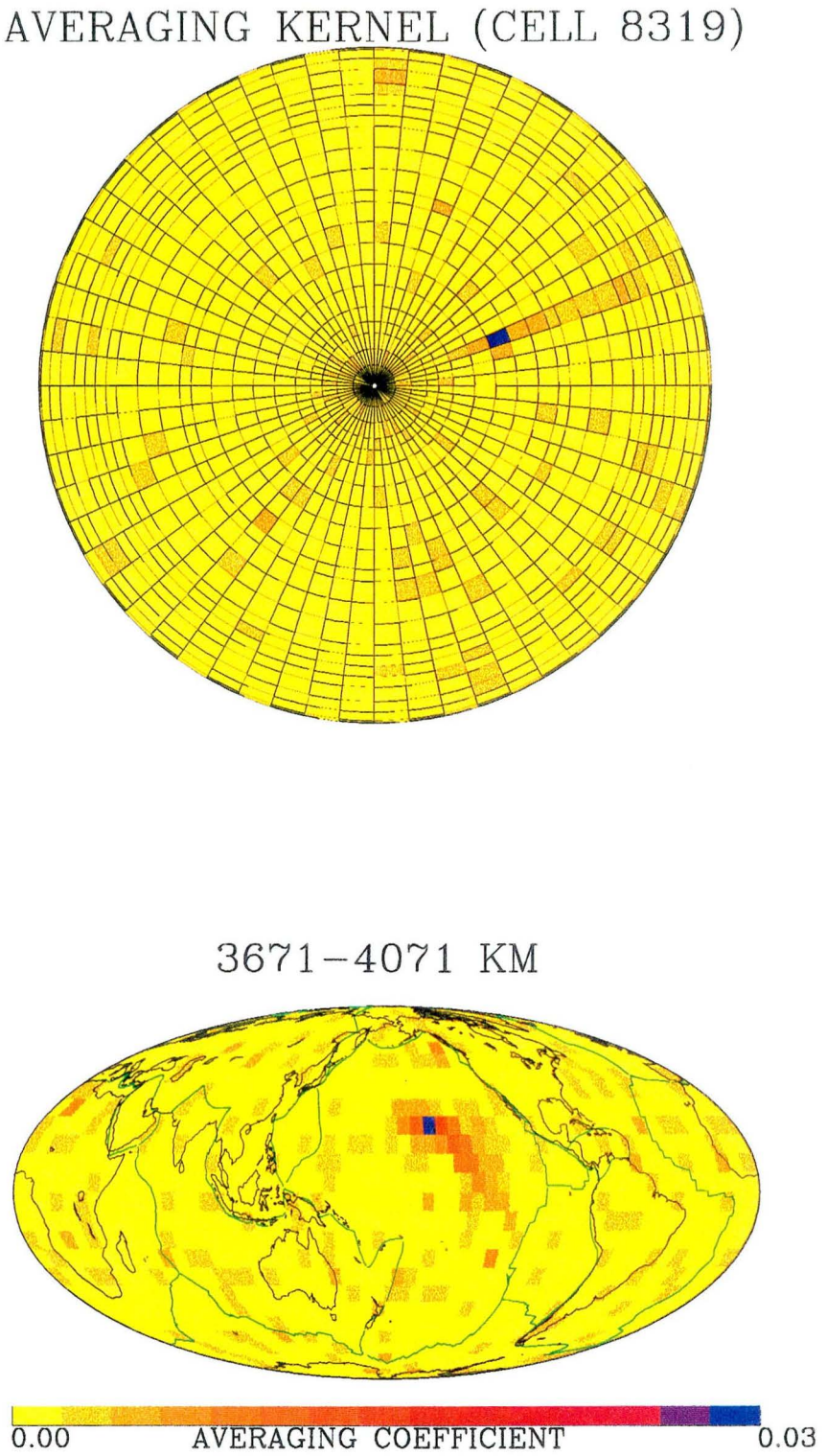
AVERAGING KERNEL (CELL 8319)
3671-4071 KM
0.00
AVERAGING COEFFICIENT
0.03

Figure 5.b

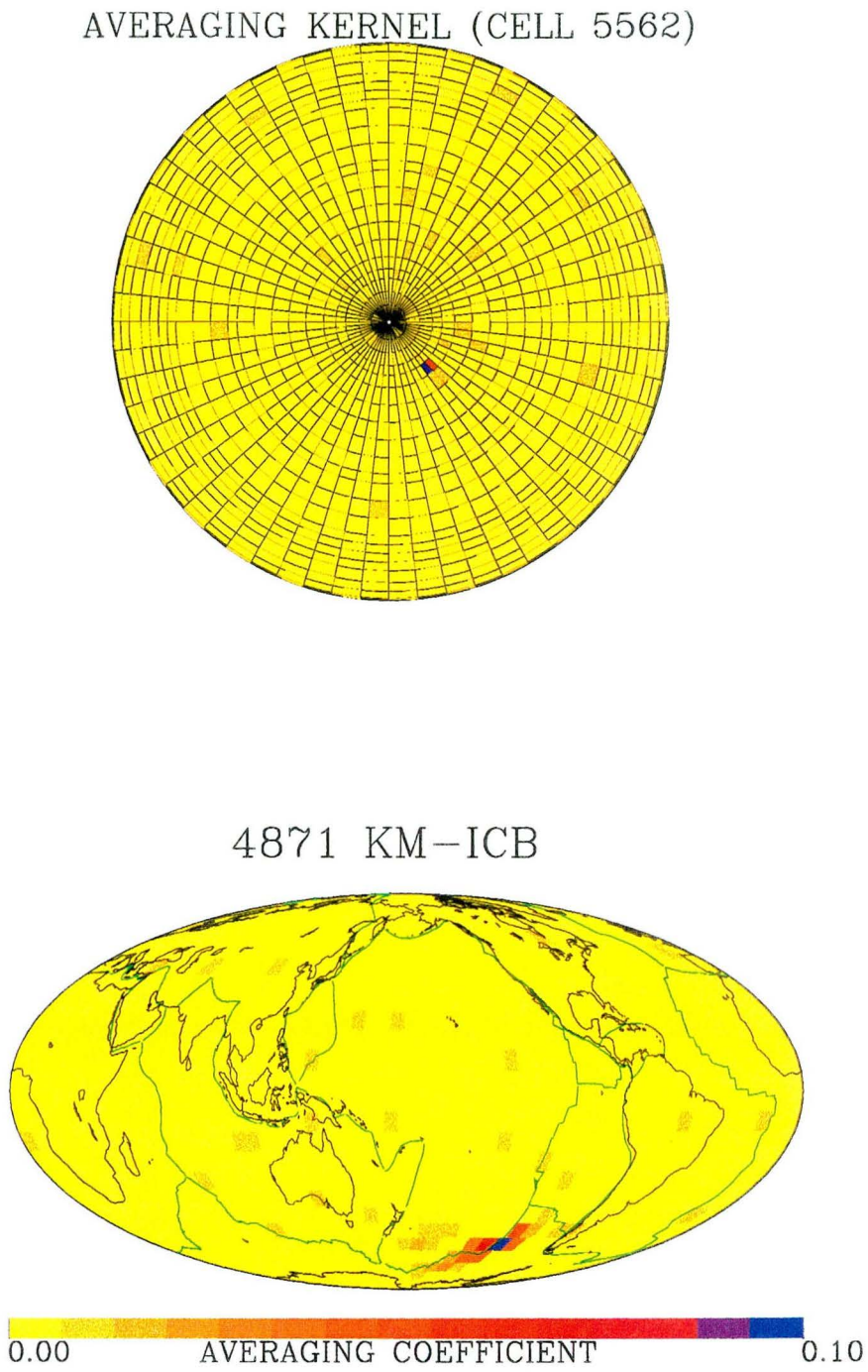
AVERAGING KERNEL (CELL 5562)
4871 KM−ICB
0.00
AVERAGING COEFFICIENT
0.10

Figure 5.c

Mantle - Compressional

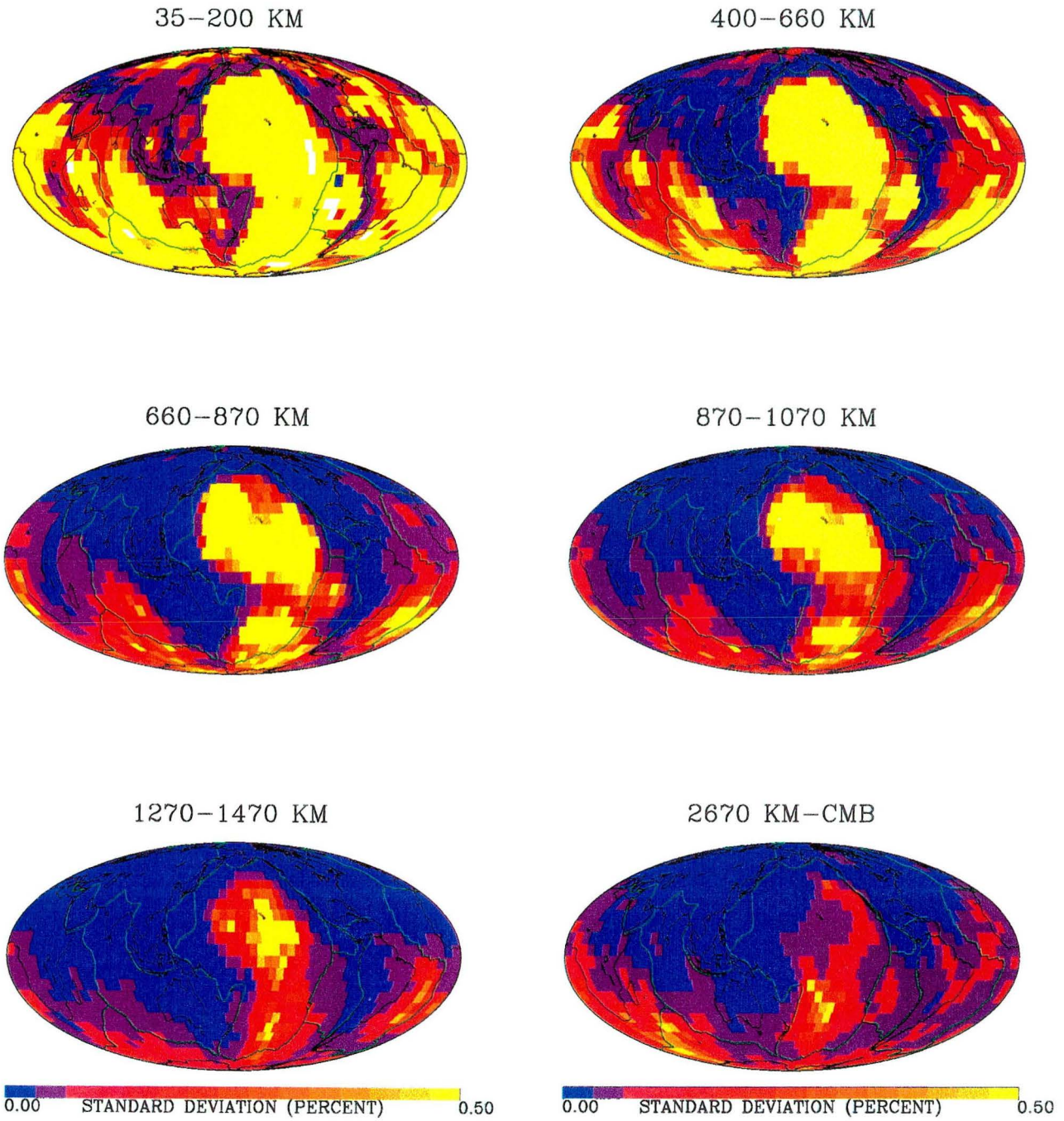

Figure 6.a

Outer Core - Compressional

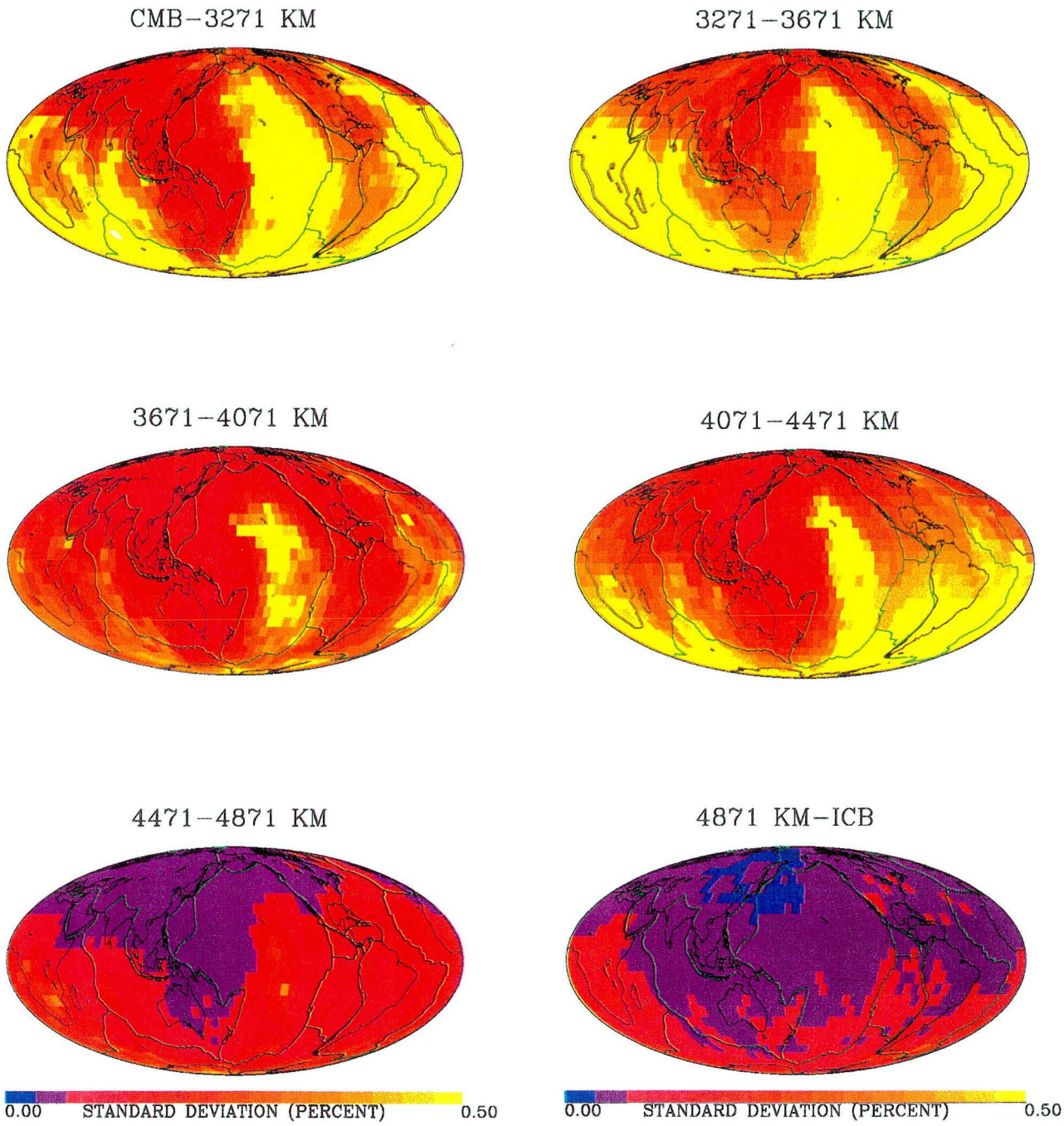

Figure 6.b

Inner Core - Compressional

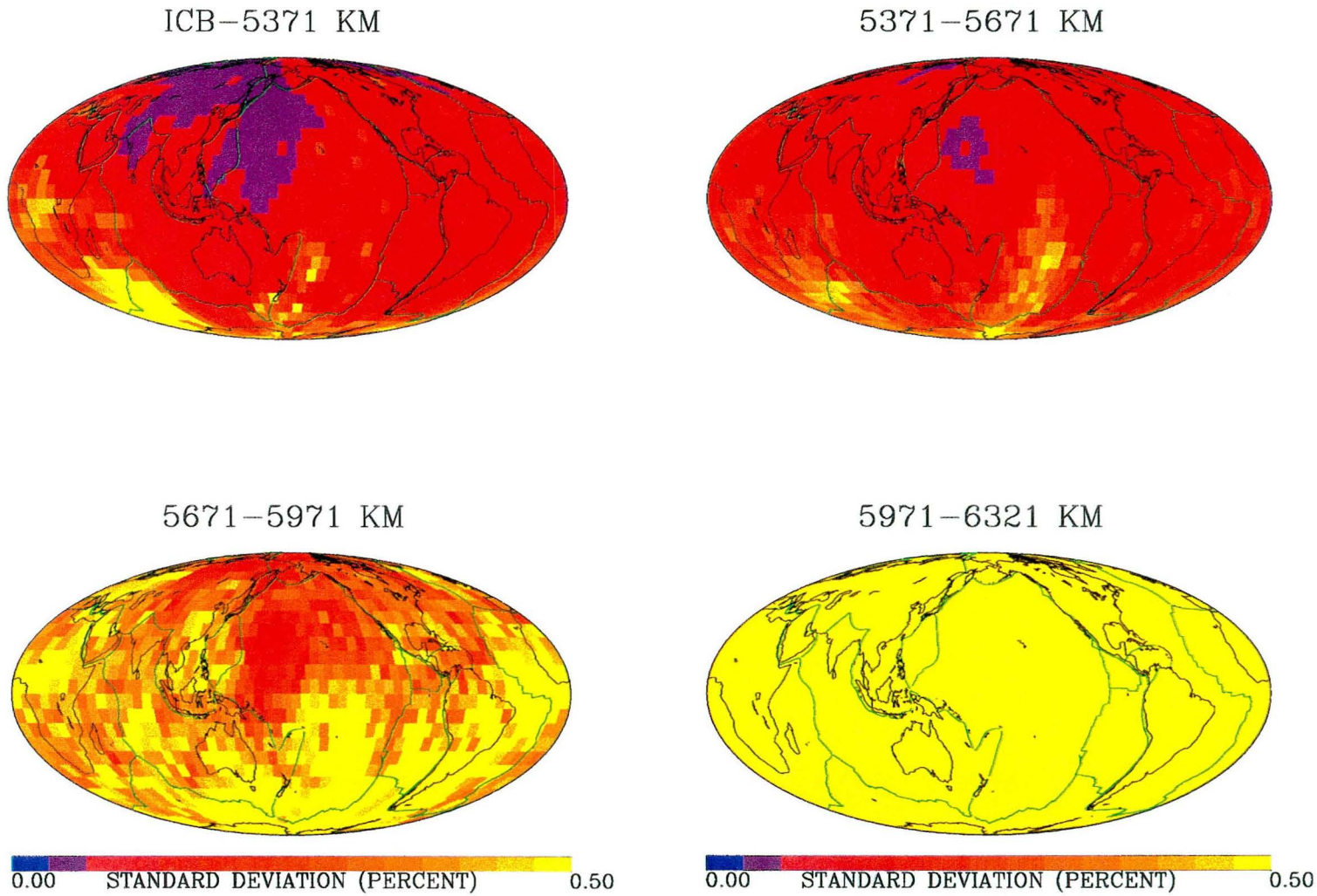

Figure 6.c

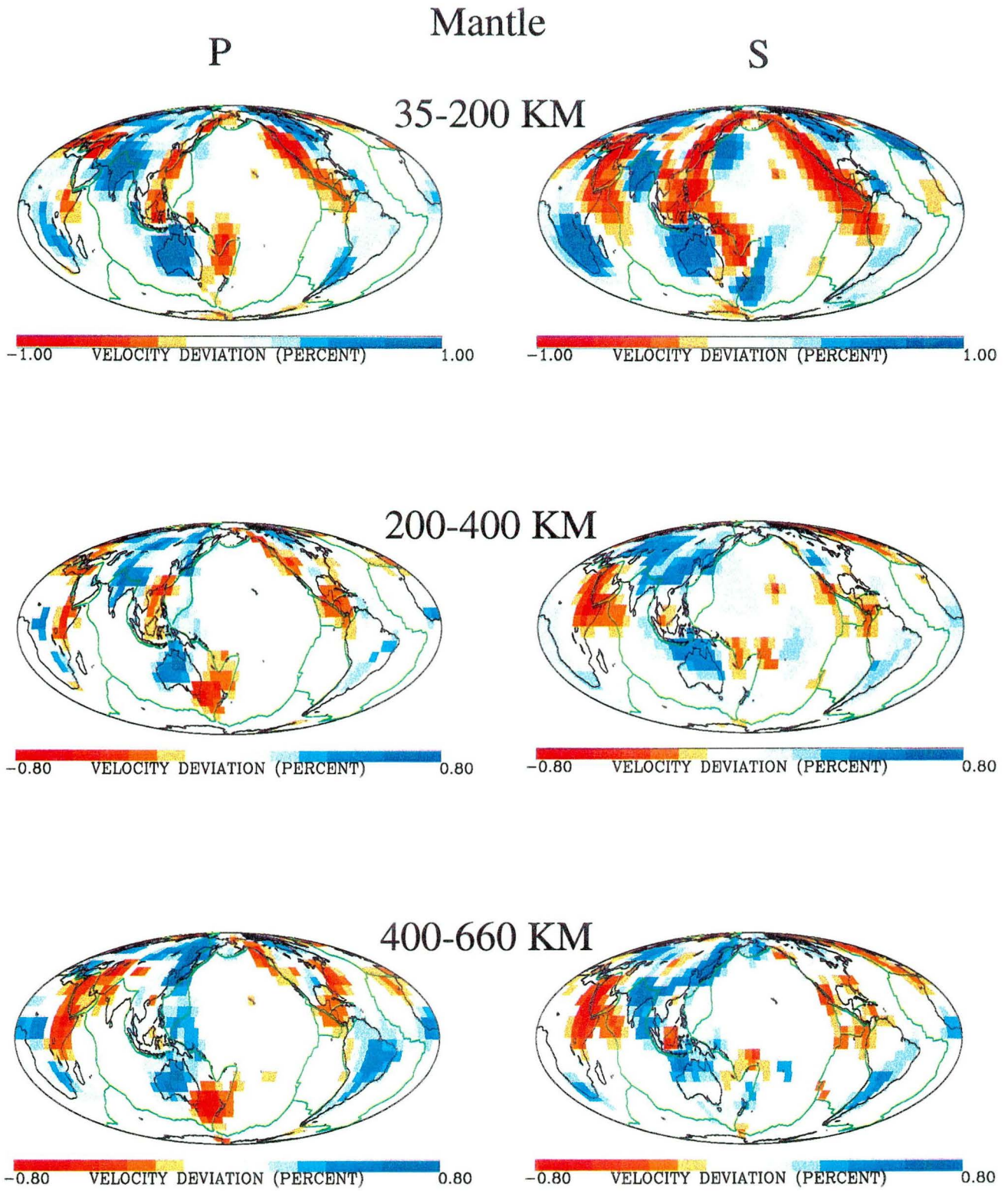
Mantle
P
S
35-200 KM
−1.00 VELOCITY DEVIATION (PERCENT) 1.00
−1.00 VELOCITY DEVIATION (PERCENT) 1.00
200-400 KM
−0.80 VELOCITY DEVIATION (PERCENT) 0.80
−0.80 VELOCITY DEVIATION (PERCENT) 0.80
400-660 KM
−0.80 VELOCITY DEVIATION (PERCENT) 0.80
−0.80 VELOCITY DEVIATION (PERCENT) 0.80

Figure 7.a

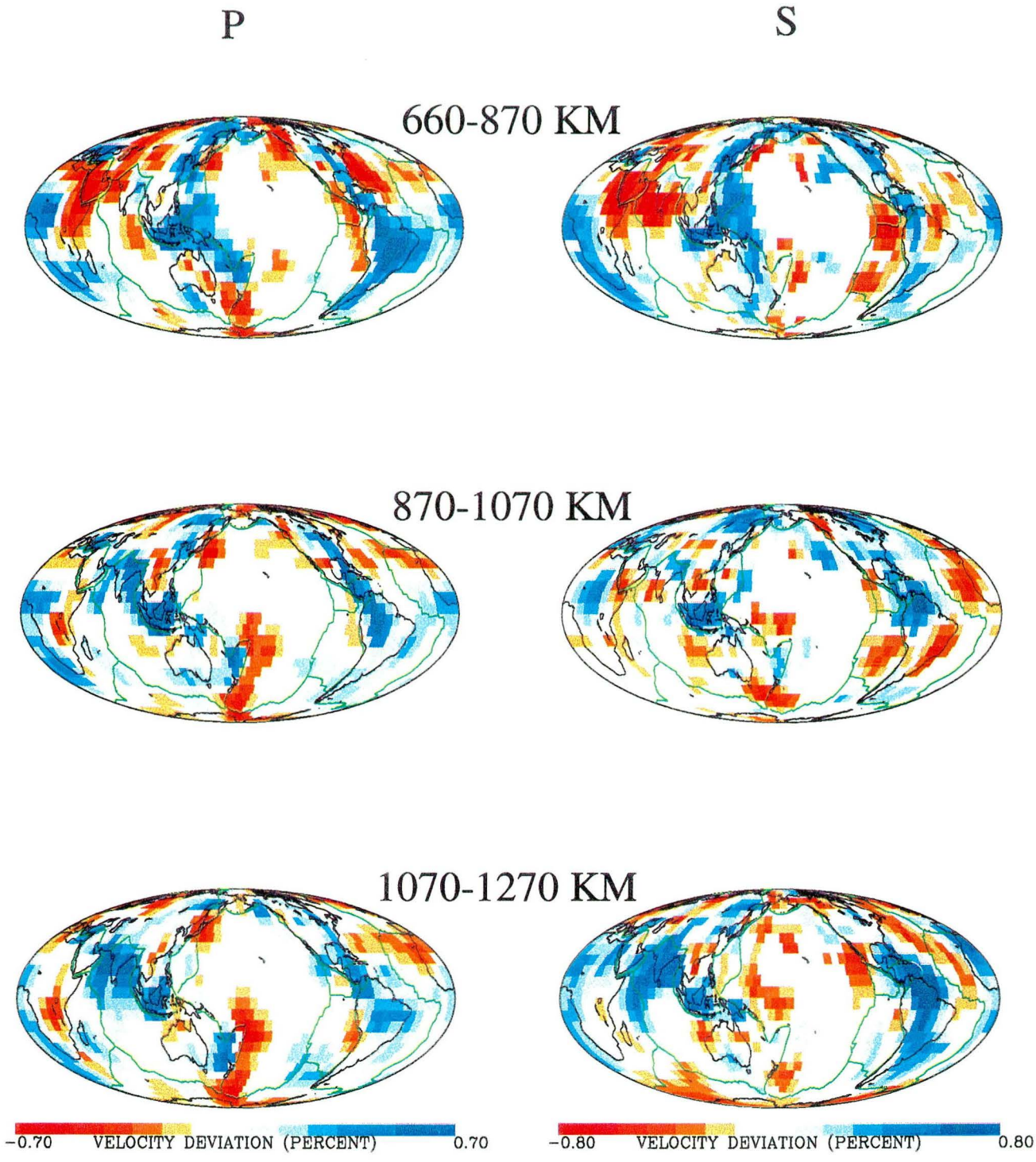
P
S
660-870 KM
870-1070 KM
1070-1270 KM
-0.70 VELOCITY DEVIATION (PERCENT) 0.70
-0.80 VELOCITY DEVIATION (PERCENT) 0.80

Figure 7.b

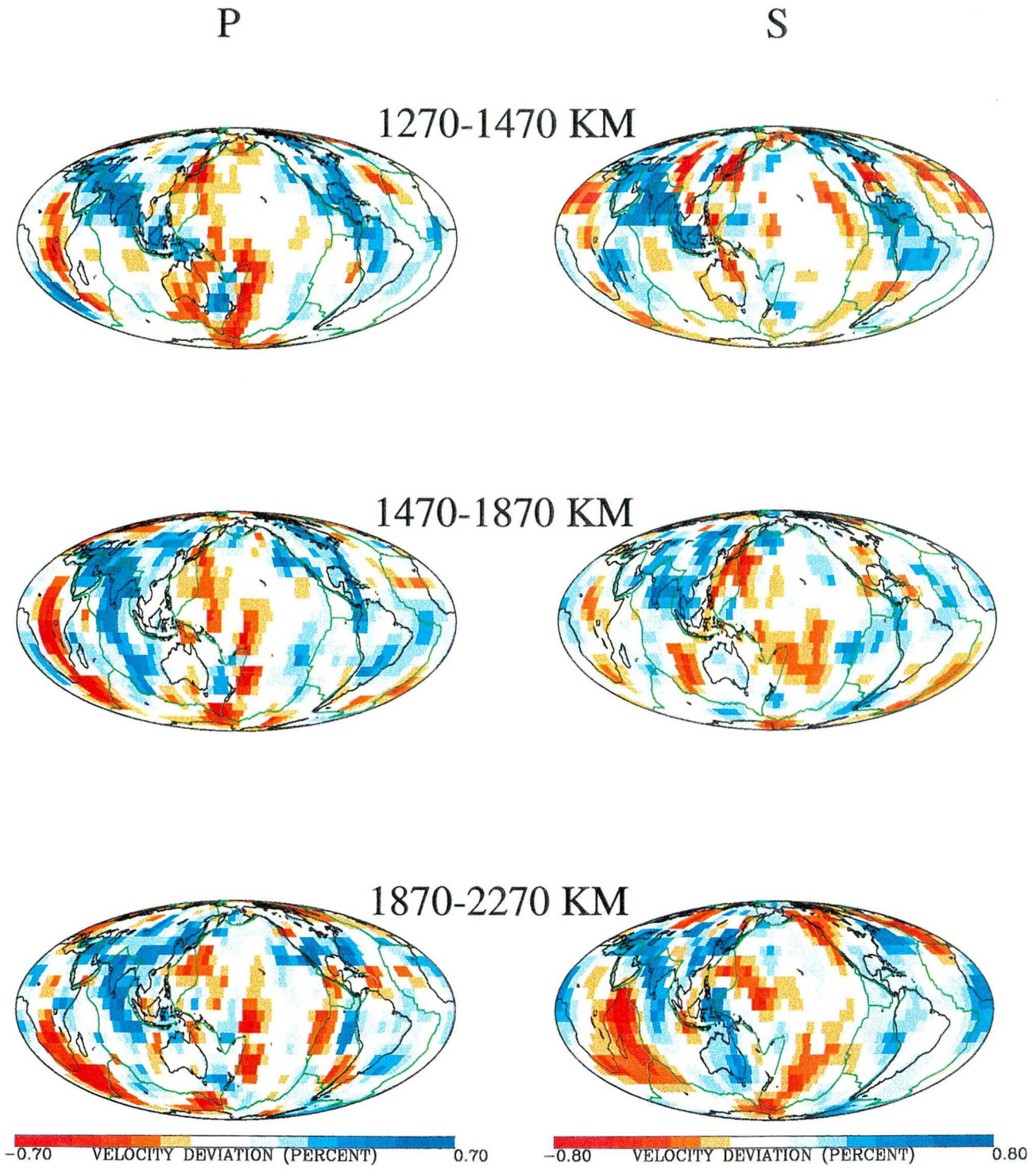
P
S
1270-1470 KM
1470-1870 KM
1870-2270 KM
-0.70
VELOCITY DEVIATION (PERCENT)
0.70
-0.80
VELOCITY DEVIATION (PERCENT)
0.80

Figure 7.c

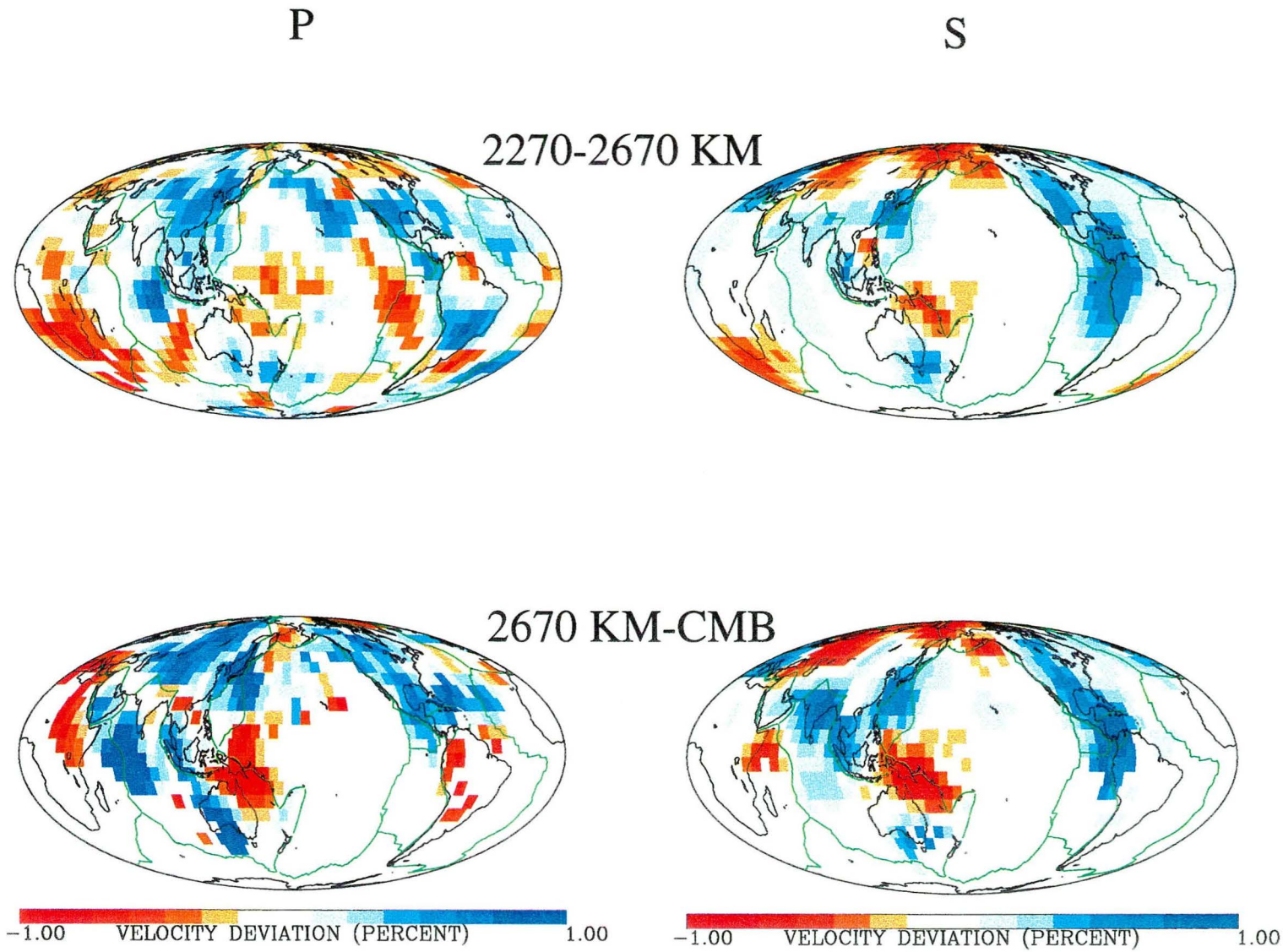
P
S
2270-2670 KM
2670 KM-CMB
−1.00
VELOCITY DEVIATION (PERCENT)
1.00
−1.00
VELOCITY DEVIATION (PERCENT)
1.00

Figure 7.d

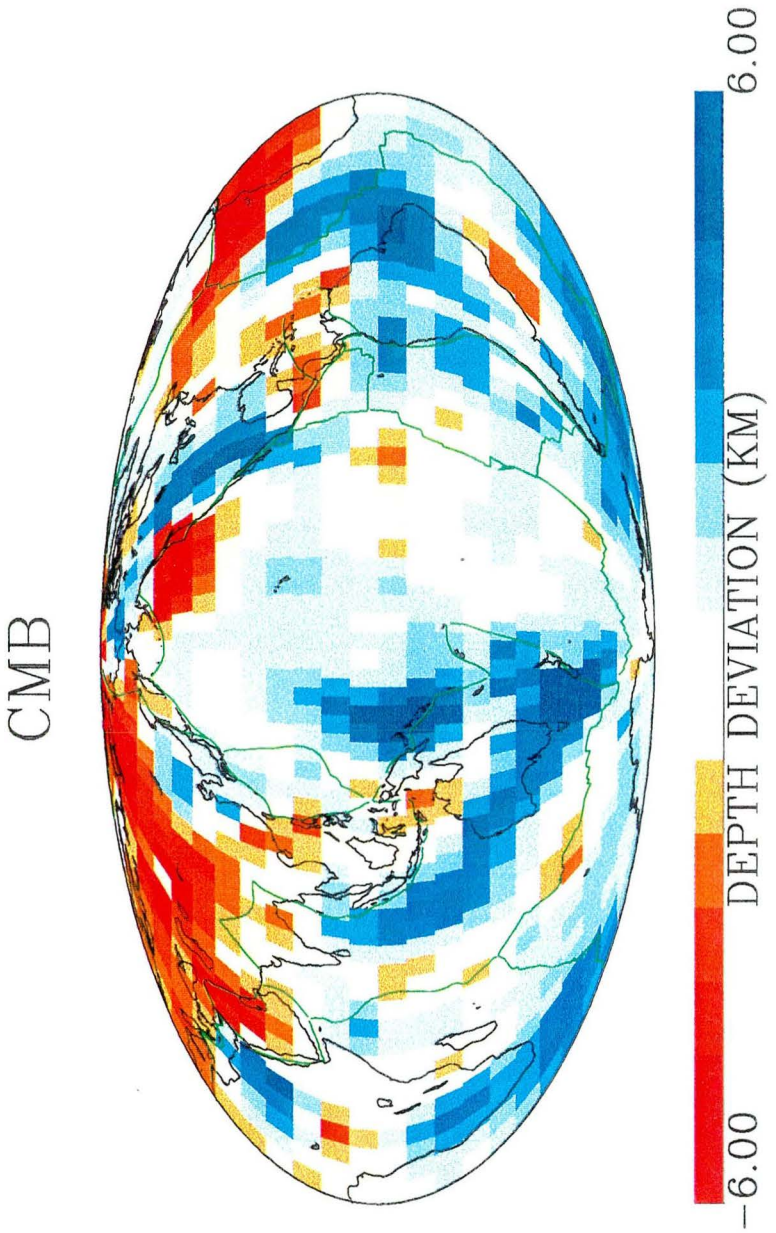

Figure 7.e

Outer Core

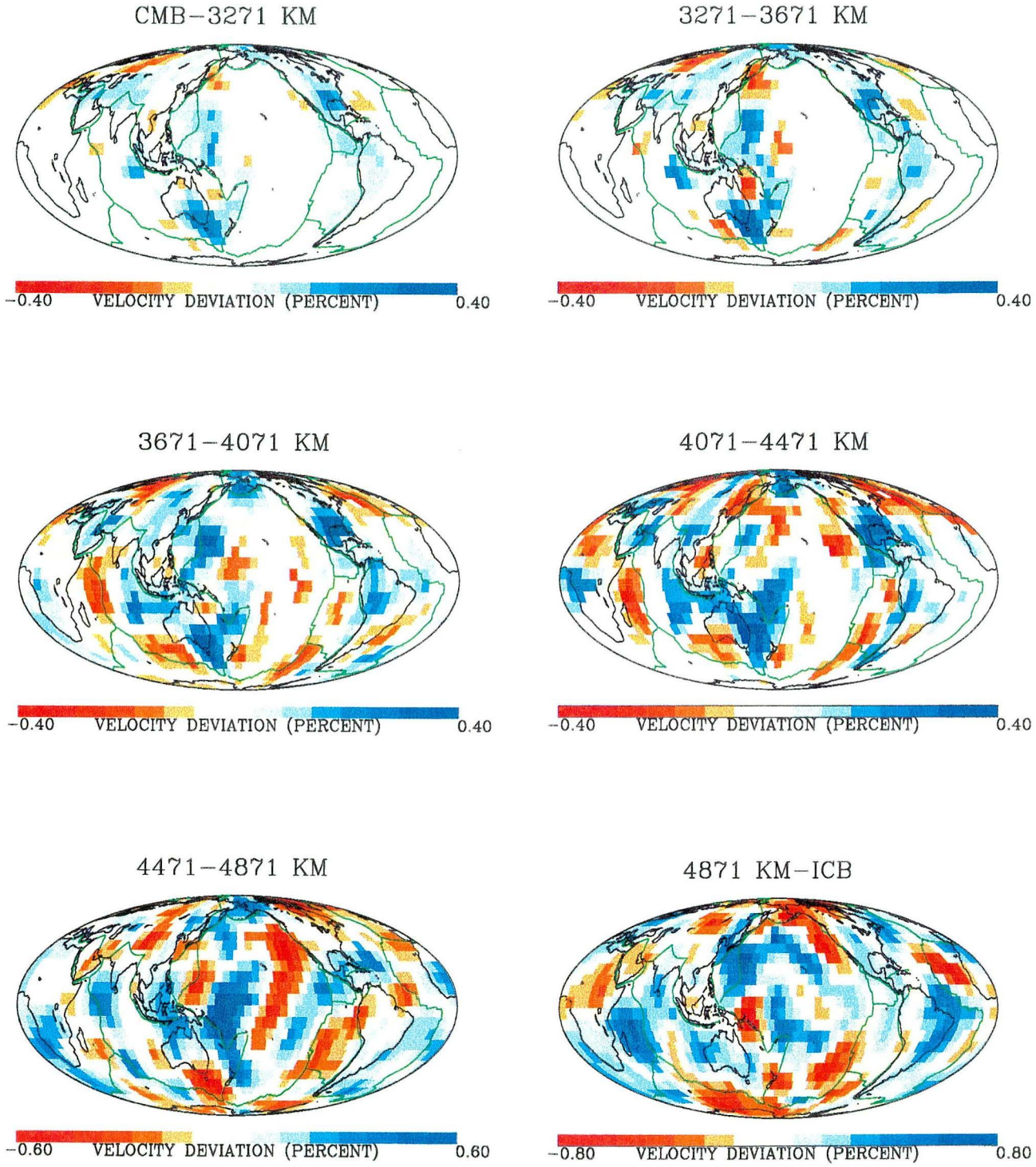

Figure 7.f

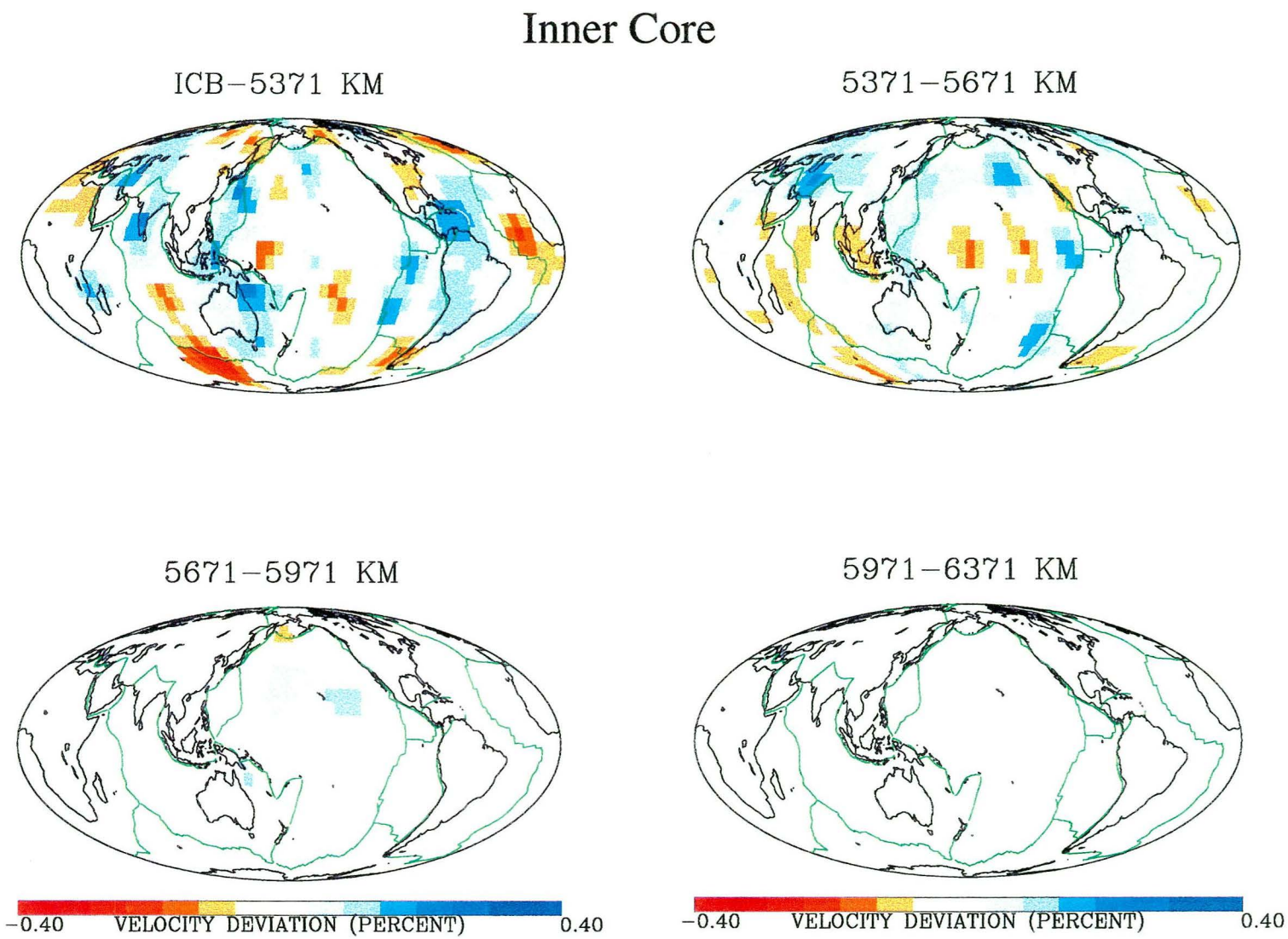
Inner Core
ICB−5371 KM
5371−5671 KM
5671−5971 KM
5971−6371 KM
−0.40
VELOCITY DEVIATION (PERCENT)
0.40
−0.40
VELOCITY DEVIATION (PERCENT)
0.40

Figure 7.g

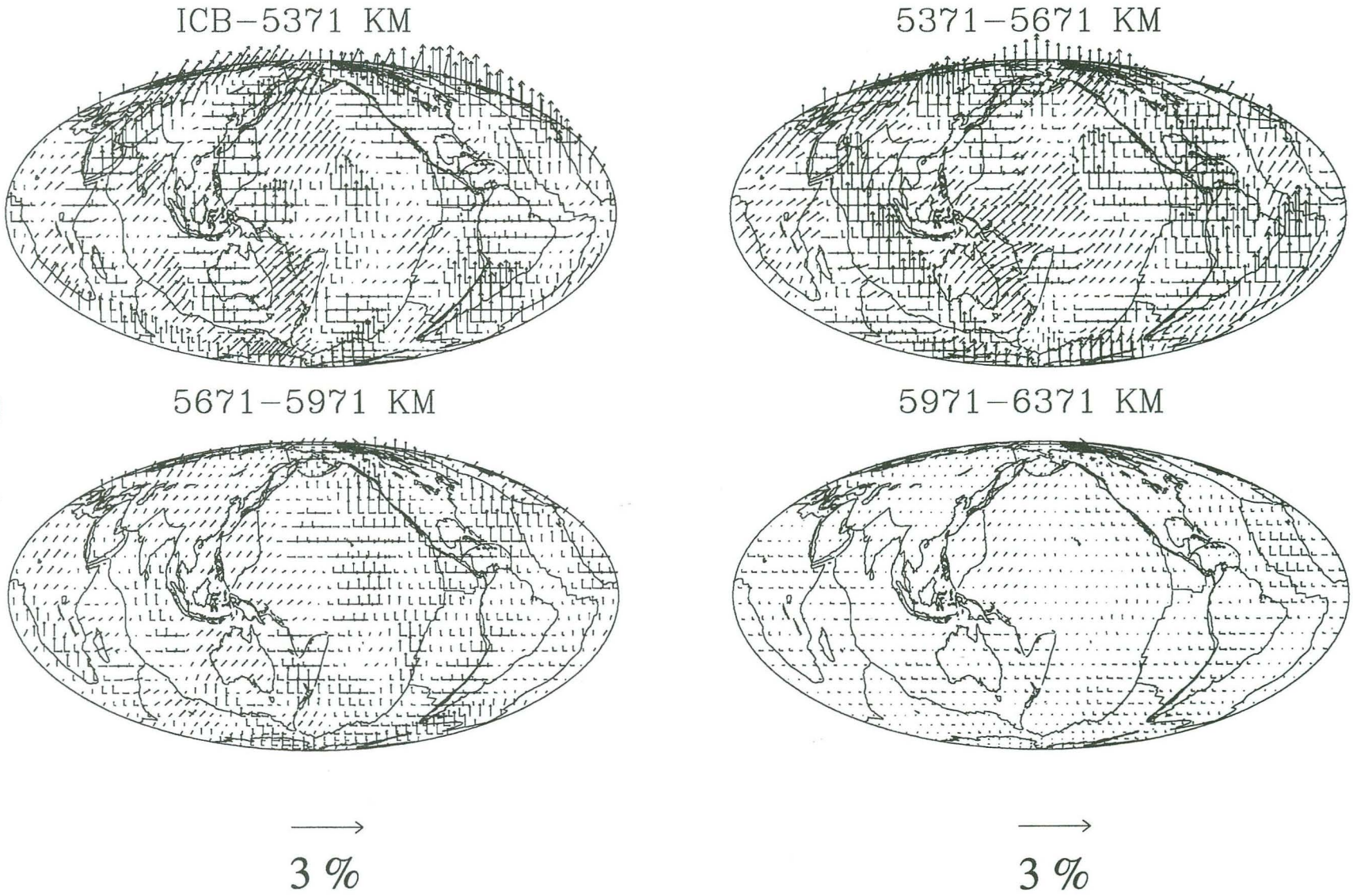

Figure 8

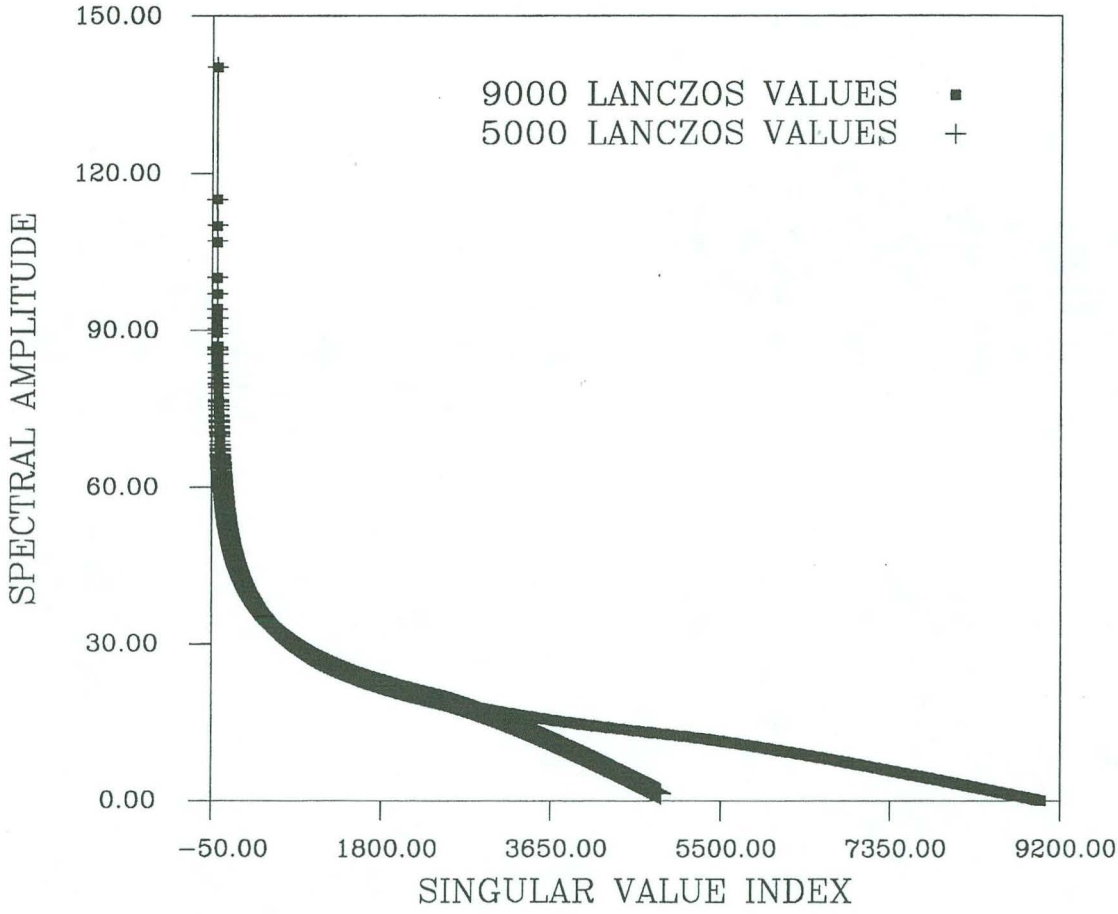
150.00
120.00
90.00
60.00
30.00
0.00
SPECTRAL AMPLITUDE
9000 LANCZOS VALUES
5000 LANCZOS VALUES
−50.00
1800.00
3650.00
5500.00
7350.00
9200.00
SINGULAR VALUE INDEX

Figure 9

Mantle - Compressional

35-200 KM

5000 LANCZOS VALUES

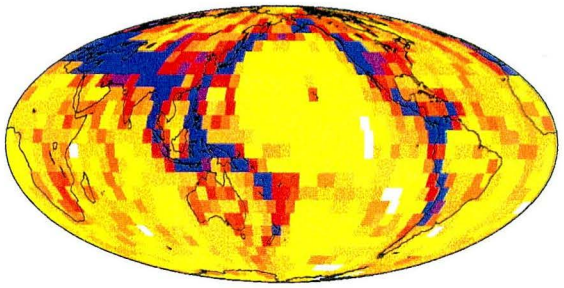

9000 LANCZOS VALUES

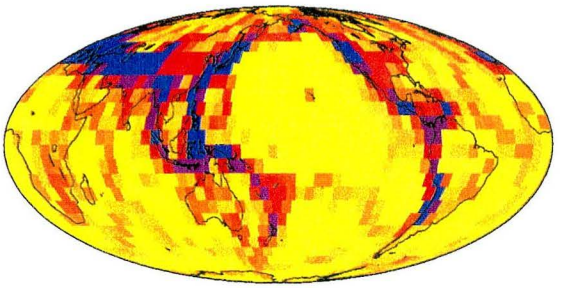

660-870 KM

5000 LANCZOS VALUES

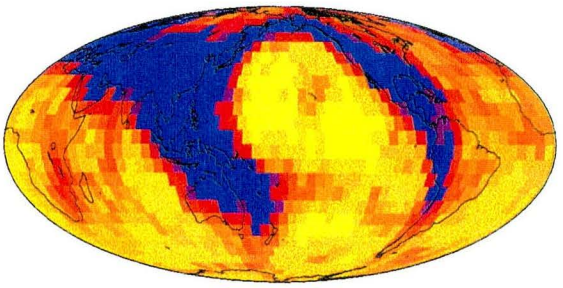

9000 LANCZOS VALUES

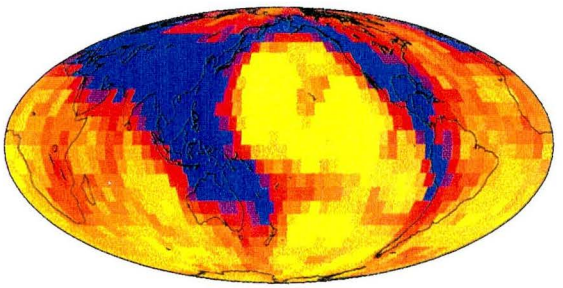

2670 KM-CMB

5000 LANCZOS VALUES

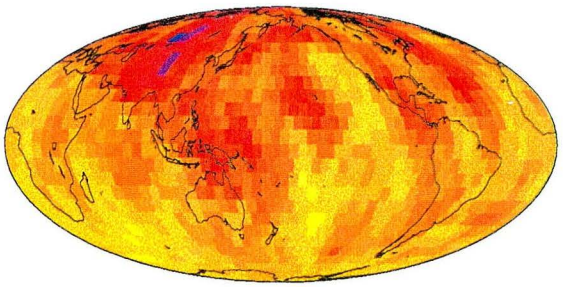

9000 LANCZOS VALUES

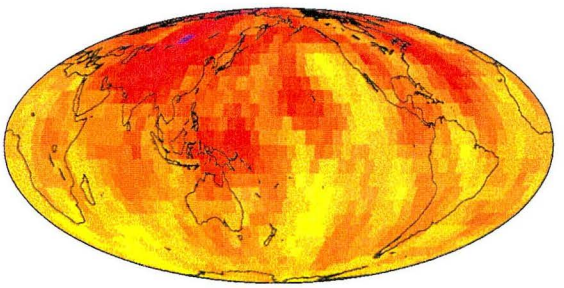

Figure 10.a

Outer Core - Compressional

CMB-3271 KM

5000 LANCZOS VALUES

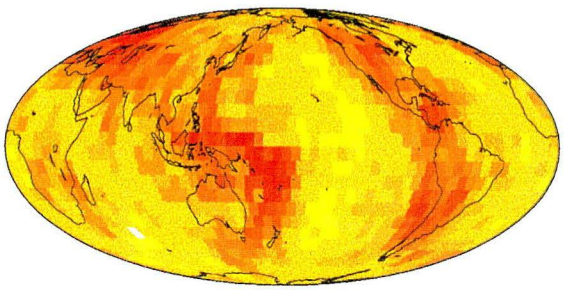

9000 LANCZOS VALUES

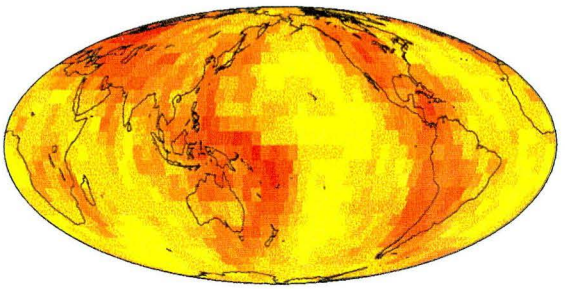

3671-4071 KM

5000 LANCZOS VALUES

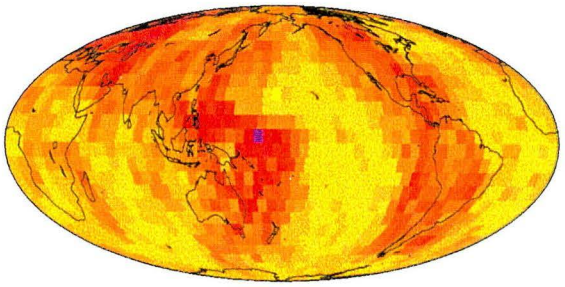

9000 LANCZOS VALUES

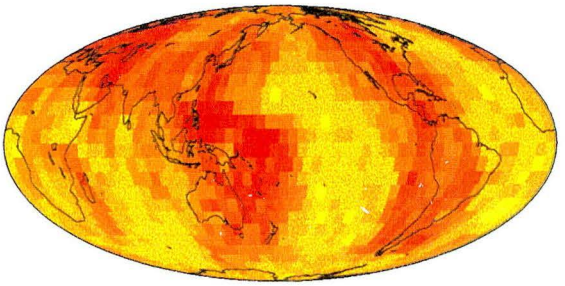

4871 KM-ICB

5000 LANCZOS VALUES

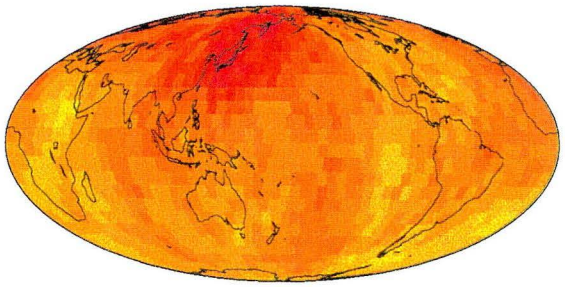

9000 LANCZOS VALUES

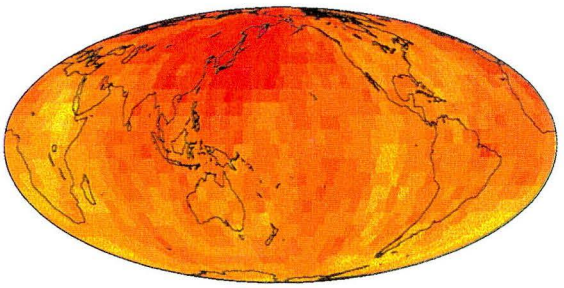

0.00 RESOLUTION 1.00

0.00 RESOLUTION 1.00

Figure 10.b

Ernest Orlando Lawrence Berkeley National Laboratory
One Cyclotron Road | Berkeley, California 94720

Prepared for the U.S. Department of Energy under Contract No. DE-AC03-76SF00098